Environmental Science

AIMS Environmental Science, 10(6): 764–793.
DOI: 10.3934/environsci.2023042
Received: 30 August 2023
Revised: 08 November 2023
Accepted: 20 November 2023
Published: 28 November 2023

http://www.aimspress.com/journal/environmental

Research article

Investigation of the potential effect of encapsulated metal nanoparticles on enhancement of thermophilic anaerobic digestion

Alaa E. Al-Ahmad[1], Stéphanie D. Lambert[2], Julien G. Mahy[2,3,*], Benoît Heinrichs[2], Wissal Wannoussa[1], Ludivine Tasseroul[2], Frédéric Weekers[4], Philippe Thonart[1] and Serge Hiligsmann[1,5,6,*]

[1] Centre Wallon de Biologie Industrielle, Université de Liège, Gembloux Agro-Bio Tech, Passage des Déportés 2 5030 Gembloux, Belgium
[2] Department of Chemical Engineering, B6a, Université de Liège, B-4000 Liège, Belgium
[3] Institut National de la Recherche Scientifique (INRS), Centre-Eau Terre Environnement, Université du Québec, 490, Rue de la Couronne, Québec (QC), G1K 9A9, Canada
[4] Artechno SA, Rue Camille Hubert 17, 5032, Belgium
[5] 3BIO-BioTech, Ecole Polytechnique, Université Libre de Bruxelles, Avenue F. Roosevelt, 50, CP165/61, B1050 Brussels, Belgium
[6] BioTech-Extraction Department, CELABOR Research Center, Av. du Parc 28, 4650 Herve, Belgium

* **Correspondence:** Email: julien.mahy@uliege.be; serge.hiligsmann@celabor.be.

Abstract: The present work investigates the enhancement effect of seven different catalysts made of Cu/SiO_2, Pd/SiO_2, Pt/SiO_2, Ni/SiO_2, Co/SiO_2, Ag/SiO_2 and Fe/SiO_2 nanoparticles (NPs) on methane production during thermophilic anaerobic digestion. The tested NPs were synthesized by the sol-gel process and encapsulated in porous silica (SiO_2) to prevent their coagulation and agglomeration. Transmission electron microscopy (TEM) pictures confirmed the specific morphologies of all seven catalysts.

Then, these 7 NPs were tested first in batch experiments with acetate as a carbon substrate for bio-methane production. Ni/SiO_2 and Co/SiO_2 showed the best enhancement of methane production from acetate. From this part, both NPs were tested for bio-methane production on two different substrates: starch and glucose. With the starch substrate, the improvements of methane production were equal to 47% and 22%, respectively, for Ni- and Co/SiO_2 compared to control sample. In the last part of this work, the influences of NP concentration and thermal pre-treatment applied to the NPs on bio-methane production from glucose were investigated. The results showed that all forms of nickel and cobalt NPs

enhance the methane production, and their effect increased with the increase of their concentrations. The best sample was the calcined nickel NPs at a concentration of 10^{-4} mol L^{-1}, leading to a methane production rate of 72.5% compared to the control.

Keywords: nanoparticles; heavy metal; anaerobic digestion; methane production; hydrogen; sol-gel process

1. Introduction

Increased demand and inevitable depletion of fossil fuels, together with worldwide concerns about greenhouse gas emissions, have resulted in the development of promising technologies for renewable energy production [1]. Therefore, potential alternatives for energy generation are intensively studied. One option is the use of biomass feedstock for the production of biogas through anaerobic digestion [2,3]. This process is a biochemical technological process for the treatment of a wide range of feed-stocks (e.g., organic fraction of municipal waste, animal manure and slurry, agricultural crops, etc.) to produce methane-rich biogas which can be used as a replacement for fossil fuels in both heat and power generation and as a vehicle fuel [4,5].

However, there are critical issues, which need to be addressed to make the production of bio-methane a techno-economically viable and ecologically acceptable renewable substitute. One of the most important issues is the effect of trace metals addition on anaerobic digestion. These metals can be stimulatory, inhibitory or even toxic for biochemical reactions, depending on their concentrations [6,7].

As reported in the literature, nickel [8–12], cobalt [8,11,13,14], iron [15–18] and molybdenum [19] are all involved in the methane production biochemical process and serve as cofactors in enzymes which are involved in the biochemistry of methane formation [7, 20]. In addition, a number of microbes are able to use some metals or metalloids as electron donors or acceptors in energy metabolism. They include eubacteria and archaea. Depending on the element, the metal species may be in simple ionic form or in the form of oxyanions. As energy sources, oxidizable metals or metalloids may satisfy the entire energy demand of an organism [21].

Due to nanoparticles' (NPs') (particles of 1–100 nm in diameter) unique electronic, optical, photonic and catalytic properties [22], which are primarily based on their small size and their high surface to bulk ratio, and because of their great potential in application to many science fields, the last decades have been marked by the increased attention of scientists to NPs [23,24].

Recently, enormous interest has been focused on biological application of metal NPs since they have shown interactions with microorganisms. Nevertheless, the influence of metal NPs on anaerobic digestion has seldom been investigated. Some publications discussed the effect of NPs' addition on anaerobic digestion. For example, Gonzalez-Estrella et al. [25] reported that Ag^0, Al_2O_3, Ce_2O_3, Mn_2O_3, Fe^0, Fe_2O_3, SiO_2 and TiO_2 NPs did not show any inhibitory effect on methanogens' activities even at concentrations of 1500 mg L^{-1}. Likewise, nano-TiO_2, Al_2O_3 and SiO_2 in doses up to 150 mg g^{-1} – TSS (total soluble sugars)) showed no inhibitory effect, whereas nano-ZnO showed inhibitory effect with its dosage increased [26]. Luna-delRisco et al. [27] reported that 10.7 mg L^{-1} CuO and 57.4 mg L^{-1} ZnO NPs inhibited methane production from cattle manure. Other authors investigated the enhancement effect of NPs at very low concentration on bio-hydrogen anaerobic fermentation,

including silver NPs [14,28], hematite Fe_2O_3 NPs [29,30], gold NPs [14,31], iron NPs [24,32], etc. At present, little is known about how NPs affect microorganisms in an anaerobic environment. Therefore, it is attractive to investigate the catalytic effect of NPs on methane production.

Many syntheses are reported to produce metal nanoparticles with different sizes and shapes, such as calcination/H_2 reduction [33,34], chemical reduction [35–40], photoreduction [41], bio-based reduction [42,43], sol-gel methods [44–46] or biosynthesis [47–50]. Nevertheless, the sol-gel method is one of the most versatile synthesis techniques [44–46]. This process allows the dispersion of metallic nanoparticles inside a metal oxide matrix, such as silica, thanks to modified alkoxides able to form complexes with metallic precursor [51–53]. This method was called cogelification [51,52], allowing one to avoid sintering and agglomeration of the metallic NPs. The sol-gel method uses low temperature and ambient pressure for material synthesis.

The purpose of this study was to investigate the influence of metal NPs (Cu/SiO_2, Pd/SiO_2, Pt/SiO_2, Ni/SiO_2, Co/SiO_2, Ag/SiO_2 and Fe/SiO_2) on methane generation during anaerobic digestion and to suggest the mechanisms. The novelty of this study resides in the use of metallic NPs that are encapsulated in porous silica, allowing a constant release of the metal and avoiding agglomeration of the catalysts, to enhance bio-methane production. First, the effects of these seven NPs on methane generation were studied with acetate substrate as the final intermediate used to produce methane, and the experiments were carried out in batch tests (125 mL vials). In the second step, the effects of the most efficient NPs resulting from previous assays were investigated with complex substrates such as starch and glucose with three different NP concentrations, 10^{-4}, 10^{-5} and 10^{-6} mol L^{-1}. Gas and liquid chromatography were used to monitor the intermediates and final metabolites, such as volatile fatty acids (VFAs) produced from the initial substrate of each stage.

2. Materials and methods

2.1. Synthesis of NPs

Metallic salts of Cu, Pd, Pt, Ni, Co, Ag and Fe were used for the synthesis of encapsulated NPs inside a porous silica matrix, denoted as Cu/SiO_2, Pd/SiO_2, Pt/SiO_2, Ni/SiO_2, Co/SiO_2, Ag/SiO_2 and Fe/SiO_2. The sol–gel process was used as described by [54,55]. This process consists of the following: (i) First, there is the preparation in one step (called the "cogelation" method), based on the concomitant hydrolysis and condensation of tetraethoxysilane (TEOS, $Si(OC_2H_5)_4$) with a modified alkoxide of formula $(RO)_3Si\text{-}XL$, in which the ligand L is able to form a complex $(LM)_n^{m+}$ with a metallic cation M^{m+} (such as Pd^{2+}, Ag^{+}, Pt^{2+}, ...) and is connected to the alkoxide $(RO)_3Si$- moiety through an inert and hydrolytically stable organic group, X. By this method, materials in which the metallic cation is anchored into the matrix were obtained. (ii) Then, there is drying under vacuum to remove solvent, calcination under air to burn organic moieties and reduction under hydrogen to reduce metallic oxides into metals. The samples were characterized by nitrogen adsorption-desorption isotherms, electron microscopy and X-ray diffraction, as previously described in [54,55]. For the clarity of this work, NPs are defined as metallic (dried), metallic oxide (calcined) and zero-valent metal (reduced) nanoparticles highly dispersed inside the silica matrix, whereas catalyst is used to refer the combination between NPs and silica.

Concentrated suspensions in water of these samples were prepared in 50 mL bottles by finely pounding (at micrometer-size) and weighing some catalysts. Based on the mass suspended in the bottles, the metallic mass loading in the catalyst and the metal atomic weight, a defined volume of

homogenized suspension was transferred in the culture medium prior to sterilization in order to reach a final concentration of 10^{-4} mol metal L^{-1}. Therefore, all the tests had the same NP concentration, but the total mass of catalyst (i.e., NPs + SiO_2) differed from one test to the others, because the metallic mass loading differs between the investigated catalysts.

2.2. Characterizations of NPs

Nitrogen adsorption-desorption isotherms of all NPs samples were determined in an ASAP multisampler device from Micromeritics at –196 °C.

X-ray diffraction (XRD) patterns were recorded on a Bruker D8 Twin-Twin powder diffractometer (Bruker, Billerica, MA, USA) using Cu-Kα radiation.

Transmission electron microscopy (TEM) pictures were obtained on a Tecnai G2 TWIN device from FEI.

The actual composition of the metal in the SiO_2 materials was determined by inductively coupled plasma atomic emission spectroscopy (ICP–AES), with an ICAP 6500 THERMO Scientific device. The mineralization is fully described in [56], with HF used instead of HNO_3.

2.3. Experimental conditions

The batch tests were performed in three experiments. The first experiment was aimed to study the effect of 10^{-5} mol L^{-1} of Cu/SiO_2, Pd/SiO_2, Pt/SiO_2, Ni/SiO_2, Co/SiO_2, Ag/SiO_2 and Fe/SiO_2 NPs on methane production by acetoclastic methanogens. Sodium acetate monohydrate (5 g L^{-1}) was used as a substrate. In the second experiment, soluble starch (5 g L^{-1}) was used as substrate with 10^{-5} mol L^{-1} of Ni, Co and Cu NPs. In the third experiment, the effects of different concentrations and different valence states of Ni/SiO_2 and Co/SiO_2 NPs were investigated using glucose monohydrate as the substrate. Batch studies were performed to analyze methane production of each combination during treatment. Control trials were performed without NPs.

All batch tests were conducted in triplicate in 125 mL glass serum vials containing 65 mL of nutrients (modified MDT medium) and specified concentrations of NPs (mol L^{-1}). The vials were inoculated by 5 mL of anaerobic sludge obtained from a full-scale anaerobic reactor treating bio-hydrogen effluent. The vials were capped with butyl rubber and degassed with nitrogen for 2 min to remove oxygen from the headspace and maintain an anaerobic environment. The tests were performed under thermophilic conditions (55 °C).

The modified MDT culture medium consisted of the following composition (in g L^{-1}): Casein peptone (0.5), yeast extract (0.5), $MgSO_4.7H_20$ (0.5), Na_2HPO_4 (5.1), KH_2PO_4 (1.2). Chemicals were purchased from Sigma. All of the media solution was autoclaved at 121 °C for 20 min. The pH of the medium was adjusted to 7.2 ± 0.2 using NaOH or HCl solutions.

2.4. Monitoring and analytical methods

The biogas production was measured by releasing the gas pressure in the vials using appropriately sized glass syringes in the 2.5–60 mL range to equilibrate with the ambient pressure. Water containing 9 M KOH in 100 ml gas replacement equipment was used to monitor the biogas production and composition, and the absorption potential of the KOH solution was regularly measured using gas mixtures containing 0, 20, 35, 80 and 100% carbon dioxide. The hydrogen (for the first 5 days of

fermentation), methane and carbon dioxide contents were determined for each gas sample using the procedure published by Hiligsmann et al. [57] but adapted for anaerobic digestion.

Hydrogen, methane and carbon dioxide were determined using a method described by Hamilton et al. [58]. The separation was achieved using a Hewlett Packard 5890 Series II gas chromatograph (GC; Agilent Technologies, Santa Clara, CA, USA) equipped with a 30 m long, 0.32 mm id Alltech GAS PRO GSC column (Grace, Deerfield, IL, USA) in series with a 20 m long, 0.25 mm id Chrompack CARBOPLOT P7 column (Agilent Technologies) and a thermal conductivity detector. The carrier and reference gas was He, and a mixture of nitrogen (15 %), carbon dioxide (35 %) and methane (50 %) was used to calibrate the instrument for determining the proportions of methane and carbon dioxide in the biogas. A mixture of hydrogen (80 %) and carbon dioxide (20 %) was used to allow the fraction of hydrogen in the biogas produced to be determined. The GC injection port, the thermal conductivity detector chamber and the oven were maintained at 90, 110, and 55 °C, respectively. VFAs' concentrations in the culture medium were determined using an Agilent 1110 series high performance liquid chromatograph (HPLC; Agilent Technologies) equipped with a Supelcogel C-610H column (Sigma-Aldrich, St Louis, MO, USA) preceded by a Supelguard H precolumn (Sigma-Aldrich). The columns were kept at a temperature of 40 °C, and the isocratic mobile phase was 0.1 % H_3PO_4 (in ultrapure, ''milliQ'' water), at a flow rate of 0.5 ml min^{-1}. A differential refraction index detector, kept at 35 °C, was used. This analysis took 35 min at a maximum pressure of 60 bar. The instrument was calibrated using solutions of glucose of 0.125, 0.25, 0.5, 1, 2 and 4 g L^{-1}, acetate, ethanol, propionate and butyrate. The liquid samples were collected and centrifuged at 13000 g for 10 min, and the obtained supernatants were filtered through a 0.2 mm cellulose acetate membrane (Minisart Sartorius).

2.5. Kinetic modeling

Mathematical modeling of microbial growth was been used to estimate various parameters. There are many models, such as the Gompertz, logistic, Richards, Stannard and Schnute models, that have been used for modeling somatic growth and population dynamics and therefore could be applied to microbial growth [59]. In this study, to describe the effect of NPs on anaerobic digestion and methane production, cumulative methane production curves with respect to time were initially obtained from the methane production experiments. In the next step, the modified equation of Gompertz [60] was applied to determine the methane production potential (A), maximum rate of methane production (μ_m) and the duration of the lag phase (λ). The Modified Gompertz equation (Eq 1) has been widely used to predict rates of fermentative gas production processes [61].

$$y = A \exp\left\{-\exp\left[\frac{\mu_m e}{A}(\lambda - t) + 1\right]\right\} \quad (1)$$

where y is cumulative methane production (mL), λ is lag time (day), A is methane production potential (mL), μ_m is the maximum methane production rate (mL day^{-1}), and e = 2.718281828. Values of y, λ, A and μ_m for each batch were estimated using Origin 9.0 for nonlinear regression analysis.

3. Results

3.1. Metallic NPs characterizations

The compositions of the NPs are given in Table 1. For each metallic NP, the same amount of metal

is obtained around 1 wt% (Table 1). The NP samples were measured by XRD, but due to the low amount of metal, no peak associated with the metallic species can be detected [51]. An example is given for Pt/SiO_2 NPs in Figure 1. Only the large peak corresponding to amorphous silica is noticed [51].

Table 1. Composition and specific surface area of NP samples.

Sample	Theoretical metal loading (wt%)	Actual metal loading (wt%)	S_{BET} (m^2/g)
Cu/SiO_2	1.00	0.98	285
Pd/SiO_2	1.00	1.05	310
Pt/SiO_2	1.00	1.02	560
Ni/SiO_2	1.00	0.99	305
Co/SiO_2	1.00	1.02	370
Ag/SiO_2	1.00	1.04	280
Fe/SiO_2	1.00	0.99	360

S_{BET} = specific surface area calculated with BET method from nitrogen adsorption-desorption isotherm data.

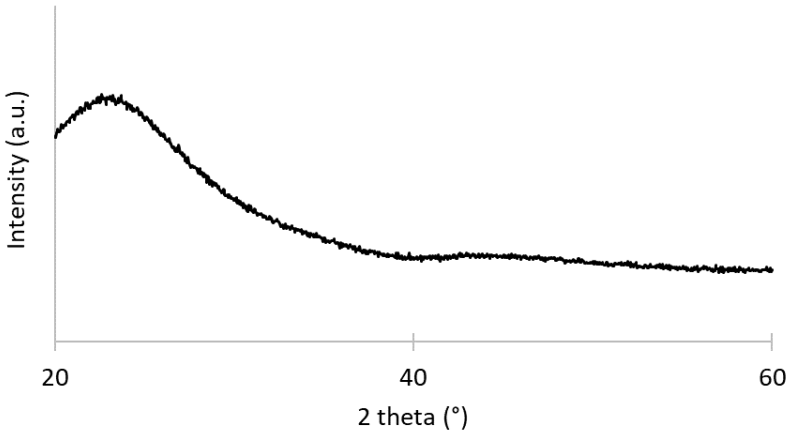

Figure 1. XRD patterns of Pt/SiO_2 sample.

The specific surface areas of all samples are also summarized in Table 1. All NP samples are in the range of 300 m^2/g, as previously observed with this amount of dopant in silica [52, 54, 62], and only the Pt/SiO_2 sample presents a higher specific surface area of 560 m^2/g.

Figure 2 presents the TEM images of all NP samples. It is observed that each sample has the same morphology: (i) They are composed of large silica nanoparticles around 20–50 nm in lighter color, and (ii) small metallic nanoparticles in dark color around 1–3 nm are dispersed in the lighter ones. This typical morphology had been observed with this specific sol-gel synthesis where small metal nanoparticles are dispersed in a porous silica matrix [52,54,62].

From these characterizations, it can be summarized that small metal nanoparticles have been highly dispersed in a porous silica matrix, allowing access to these metallic species while avoiding their agglomeration and securing a progressive metal release in water [51].

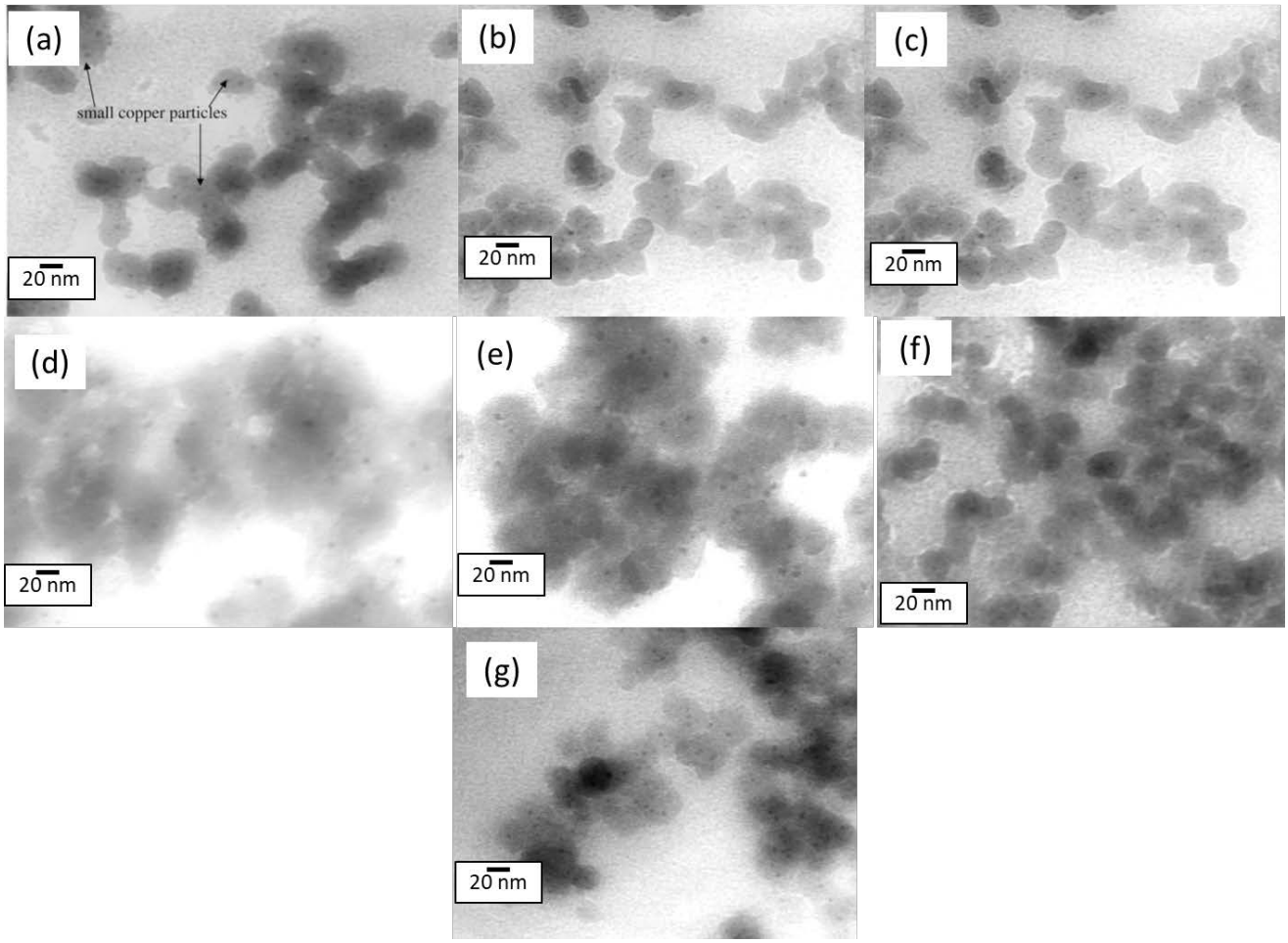

Figure 2. TEM pictures of (a) Cu/SiO_2, (b) Pd/SiO_2, (c) Pt/SiO_2, (d) Ni/SiO_2, (e) Co/SiO_2, (f) Ag/SiO_2 and (g) Fe/SiO_2 samples.

3.2. Effect of metallic NPs on acetate degradation and methane production

In a first step, seven encapsulated NPs of Cu/SiO_2, Pd/SiO_2, Pt/SiO_2, Ni/SiO_2, Co/SiO_2, Ag/SiO_2 and Fe/SiO_2 with diameters of 2–3 nm [54,55] were added in a biochemical methane potential (BMP) test (120 mL batch serum bottles with working volume of 70 mL). Sodium acetate monohydrate (5 g L^{-1}) was used as the substrate. The NP concentration was adjusted to 10^{-5} mol L^{-1} in the culture medium. The porous silica matrix used to encapsulate the NPs maintains the stability of the metal NPs, which can very easily coagulate in solution to form aggregates, which are less effective as catalysts than the original ones [63].

Biogas production was used as an indicator of anaerobic digestion imbalance [64]. The volume of biogas was measured every 15 days during 90 days after the inoculation. Cumulative methane production during the incubation period from the control and test samples with different NPs is illustrated in Figure 3. In this experiment, a slight delay in methane production occurred in all samples during the first days of fermentation due to high substrate/microorganism ratio (i.e., more substrate and less active bacteria). Hence, microbial consortia had to acclimatize to this new environment for their optimum metabolism [65]. Once the acclimatization had elapsed, the methane production started increasing in all samples and reached peak rates at 30 days specifically in the samples containing Ni/SiO_2 and Co/SiO_2 NPs, where the methane production increased significantly by 25.5 and 22.5%,

respectively, compared to the controls with substrate only. The results indicated that the addition of Ni/SiO_2 and Co/SiO_2 markedly stimulated methane production and resulted in the complete conversion of the added acetate to methane. This is in agreement with results obtained by Fathepure [66], who described the bioavailability of nickel and cobalt as an important factor for enhancement of methane production. Cu/SiO_2 and Fe/SiO_2 NPs showed a slight improvement effect on methane production, which was evident after 45 days of fermentation. Previous results [66] indicated that addition of iron at a concentration as low as 10^{-4} mol L^{-1} stimulates the conversion of acetate to methane. Furthermore, the results showed that the addition of Pt/SiO_2 and Cu/SiO_2 NPs did not have any significant effect on the production of methane and acetate consumption compared with control. The effect of copper on fermentative methane production has been documented in the literature [67,68], with a highly toxic effect on methane. However, the toxic effect of Cu/SiO_2 NPs did not appear in our experiment since NPs are encapsulated inside the porous silica matrix, which limits the metal ions' liberation. The used concentration was at the same order as that reported by Karri et al. [68], who found partial inhibition of methane production by acetoclastic methanogens at 1.6×10^{-4}– 3.2×10^{-4} mol L^{-1} of Cu^{2+} and complete inhibition at a concentration of 4.7×10^{-4} mol L^{-1} of Cu^{2+}.

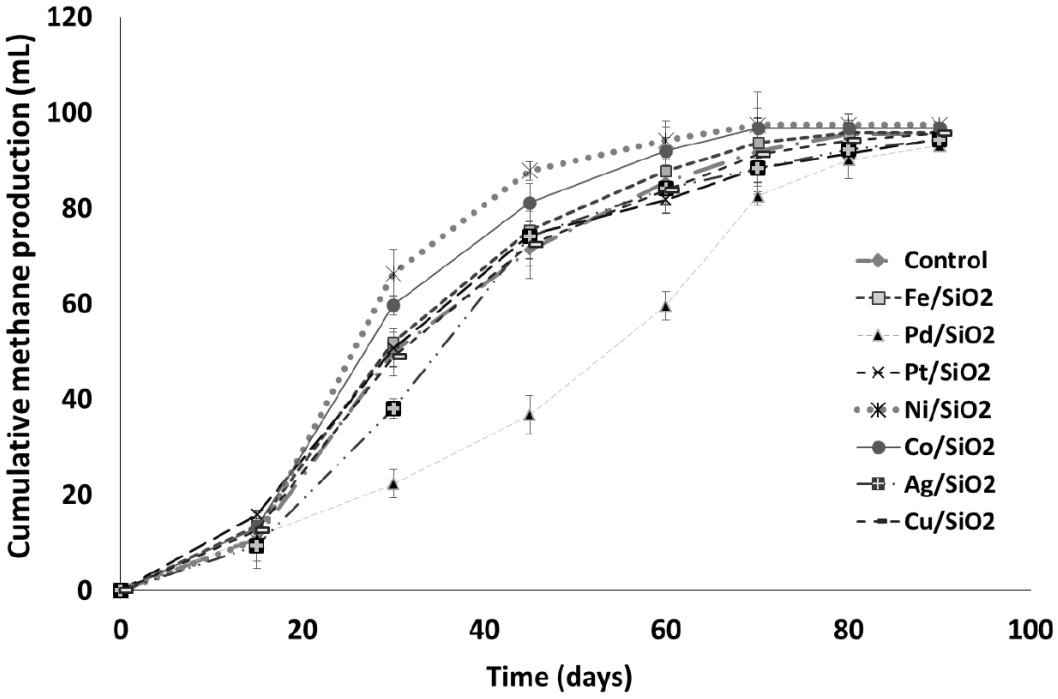

Figure 3. Cumulative volume of methane produced during thermophilic anaerobic digestion of 5 g L^{-1} acetate monohydrate in batch test (serum vials 125 mL) with 10^{-5} mol L^{-1} of encapsulated metal NPs of Cu/SiO_2, Pd/SiO_2, Pt/SiO_2, Ni/SiO_2, Co/SiO_2, Ag/SiO_2 and Fe/SiO_2. The standard deviation bars are calculated based on the triplicate experiments made for each condition.

Despite extensive use of silver NPs for antimicrobial applications, in the bottles containing Ag/SiO_2 NPs, methane production rate was a little bit slower than in control bottles, especially from the beginning until 30 days of fermentation, where methane production started to increase significantly to produce a volume of methane close to the control. The results of [69] showed that silver up to 9.10^{-4} mol L^{-1} did not adversely affect the methanogenic cultures. In contrast, it was found that Pd/SiO_2

NPs showed a clearly inhibitory effect on methane production and bacterial activity.

In order to evaluate the effects of Cu/SiO_2, Pd/SiO_2, Pt/SiO_2, Ni/SiO_2, Co/SiO_2, Ag/SiO_2 and Fe/SiO_2 NPs on methane production by acetotrophic methanogens' activity along with acetate degradation, the experimentally obtained data were fitted to the modified Gompertz model. The estimated values of the parameters are summarized in Table 2. The correlation coefficients of nonlinear analysis for all metals were above 0.99. According to this model, the values of the maximum cumulative methane productions (mL) for all samples were convergent at the end of the experiment, i.e., 95.8 ± 1.3 ml. However, the values of the maximum methane production rate (MPR) were significantly differentiated. They were 70%, 48%, 7% and 6% higher with Ni/SiO_2, Co/SiO_2, Fe/SiO_2 and Pt/SiO_2 NPs, respectively, than the control without NPs. In contrast, a significant inhibitory effect was found with Pd/SiO_2 NPs, with the maximum being 39% lower than in the control. Again, no significant inhibitory effect was found with Ag/SiO_2 and Co/SiO_2 NPs. The calculated lag time ranged between 8.03 and 16.65 days. The maximum of 16.65 days obtained for Pd/SiO_2 NPs confirms the inhibitory effect.

Table 2. Kinetic parameters and Gompertz coefficient adjusted on the profiles of volumetric methane production curves for the BMP tests with 10^{-5} mol L^{-1} of NPs and 5 g L^{-1} acetate monohydrate.

	λ (days)	μm (mL day^{-1})	A (mL)	R^2
Control	10.3±1.2	2.37±0.05	96.5±1.2	0.999
Fe/SiO_2	9.8±0.9	2.53±0.12	96.7±0.9	1
Pd/SiO_2	16.7±1.5	1.45±0.14	96.5±1.1	0.994
Pt/SiO_2	8.0±1.1	2.50±0.04	93.2±1.0	0.999
Ni/SiO_2	12.9±1.3	4.02±0.22	96.8±0.8	1
Co/SiO_2	11.7±1.0	3.50±0.08	96.7±1.0	1
Ag/SiO_2	13.9±1.3	2.27±0.09	94.3±1.8	0.999
Cu/SiO_2	9.6±0.9	2.29±0.06	96.1±0.7	0.999

Note: λ = Lag phase duration (days), μm = Maximum methane production rate (mL day^{-1}), A = Total methane production (mL), R^2 = correlation coefficient. Standard deviations are calculated based on the triplicate experiments made for each condition. All the R^2 values for the Gompertz model were higher than 0.99.

In our experiment, the production of methane is accompanied by acetate degradation. Thus, acetate concentration is a useful indicator for monitoring methane production. Figure 4 showed a significant variation in the rate of acetate degradation in the presence of NPs. The highest acetate removal rate was between 15 and 45 days, where 60–79% of acetate was converted to methane and carbon dioxide, except for the Pd/SiO_2 NPs, which showed an inhibitory effect on acetate degradation. Results indicate that Ni/SiO_2 NPs had the best effect on acetate consumption, since the acetate was depleted after 60 days. The other NPs, except Co/SiO_2 NPs, showed no significant effect on acetate degradation.

After the 90 days of culture and total arrest of methane production in all bottles, a new culture phase was carried out by adding 10 mL of acetate solution up to 5 g L^{-1} of acetate monohydrate in all serum bottles. The purpose of this experiment was to investigate the long-term effect of nanoparticles on methane production from acetate and to confirm the previous results. The results (Figure 5) showed that except for the Pd/SiO_2 NPs, the curve profiles and the volumes of methane produced during both culture phases are similar. This was confirmed when comparing the parameters of the Gompertz model

(Table 3) since no significant difference was observed between the tested NPs and the control. The values of the maximum methane production rates and lag times for all conditions were slightly lower than obtained from the first culture phase, probably due to the large inoculum in the second phase. The highest performances for methane production were recorded with Ni/SiO_2 NPs, with maximum methane production rates 69% higher than the control without NPs.

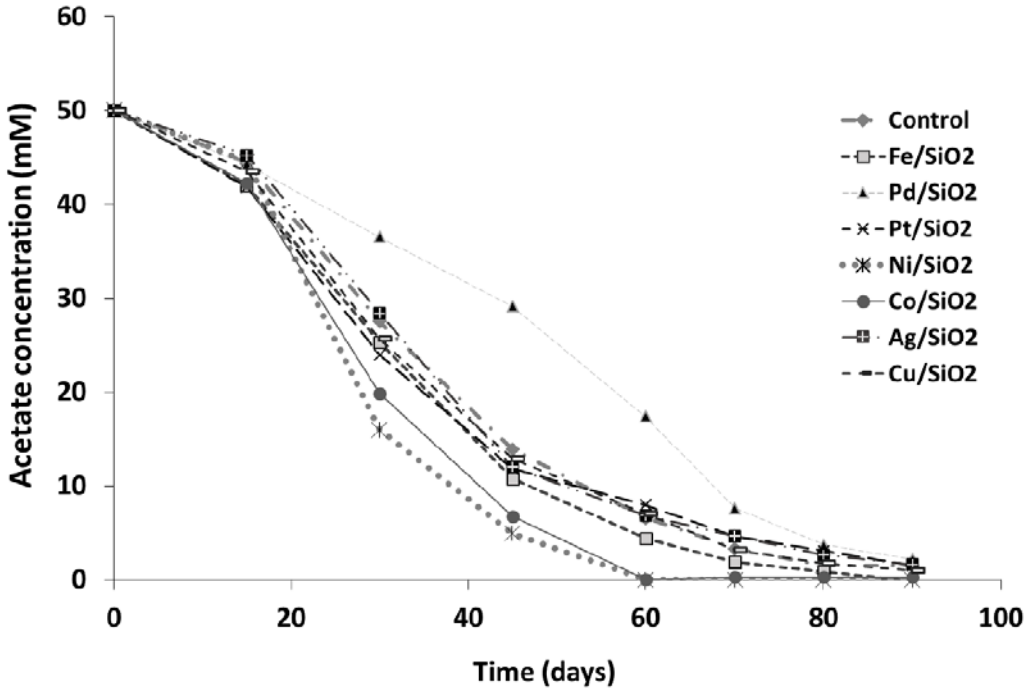

Figure 4. Evolution of acetate concentration (mM) during thermophilic anaerobic digestion of 5 g L^{-1} acetate monohydrate with 10^{-5} mol L^{-1} of encapsulated metal NPs of Cu/SiO_2, Pd/SiO_2, Pt/SiO_2, Ni/SiO_2, Co/SiO_2, Ag/SiO_2 and Fe/SiO_2.

Table 3. Kinetic parameters and Gompertz coefficient adjusted on the profiles of volumetric methane production curves for the BMP tests with 10^{-5} mol L^{-1} of NPs and the addition of 5 g L^{-1} acetate monohydrate.

	λ (days)	μm (mL day^{-1})	A (mL)	R^2
Control	6.8±0.9	1.96±0.06	93.0±2.1	0.9992
Fe/SiO_2	7.3±0.6	2.36±0.04	93.7±1.1	0.9997
Pd/SiO_2	5.3±1.1	1.49±0.17	77.2±3.4	0.9981
Pt/SiO_2	7.2±0.7	2.15±0.06	89.8±2.1	0.9984
Ni/SiO_2	7.9±0.8	3.31±0.11	93.0±2.2	0.9997
Co/SiO_2	9.3±1.1	3.13±0.09	93.3±1.9	0.9996
Ag/SiO_2	9.2±0.9	2.10±0.04	91.5±1.5	0.9995
Cu/SiO_2	8.0±0.6	2.13±0.07	91.5±1.8	0.9995

Standard deviations are calculated based on the triplicate experiments made for each condition.

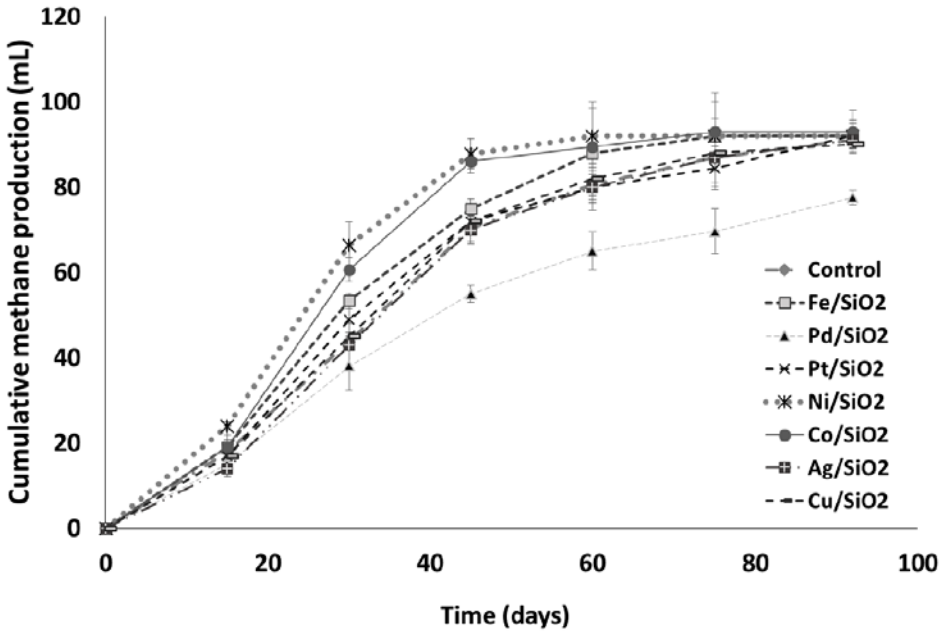

Figure 5. Cumulative volume of methane produced during second successive thermophilic anaerobic digestion of 5 g L^{-1} acetate monohydrate in batch test (serum vials 125 mL) with 10^{-5} mol L^{-1} of encapsulated metal NPs of Cu/SiO_2, Pd/SiO_2, Pt/SiO_2, Ni/SiO_2, Co/SiO_2, Ag/SiO_2 and Fe/SiO_2. The standard deviation bars are calculated based on the triplicate experiments made for each condition.

3.3. Effect of Ni/SiO_2, Co/SiO_2 and Cu/SiO_2 NPs on anaerobic digestion of starch and methane production

In consecutive experiments, Ni/SiO_2, Co/SiO_2 and Cu/SiO_2 NPs were added at the same concentration (10^{-5} mol L^{-1}) in batch cultures with 5 g L^{-1} of soluble starch as substrate. In the first 5 days of incubation, starch degradation to VFAs was accompanied by hydrogen and carbon dioxide production. Total biogas produced during the acidogenic phase (Figure 6a) was, on average, 55 mL, including hydrogen production ranging between 40 and 44 mL. This volume of hydrogen, which was eliminated, might produce 10 mL of methane by carbon dioxide reduction. However, the results displayed in Figure 6b confirmed the large influence of Ni/SiO_2 and Co/SiO_2 NPs on methane production compared to the control with substrate only. It was found that after 42 days, the addition of Ni/SiO_2 and Co/SiO_2 NPs increased the methane production by 47% and 22%, respectively, compared to the control with substrate only. Meanwhile, the addition of Cu/SiO_2 NPs showed consistently negative responses, including decrease in methane production by 6% compared with the control. The results of this work could be compared to those obtained by Pobeheim et al. [8], who found that nickel at 10.6×10^{-6} mol L^{-1} enhanced methane production by 25%, and cobalt at 2×10^{-6} mol L^{-1} increased the methane production by 10% approximately from substrate consisting of xylan and starch.

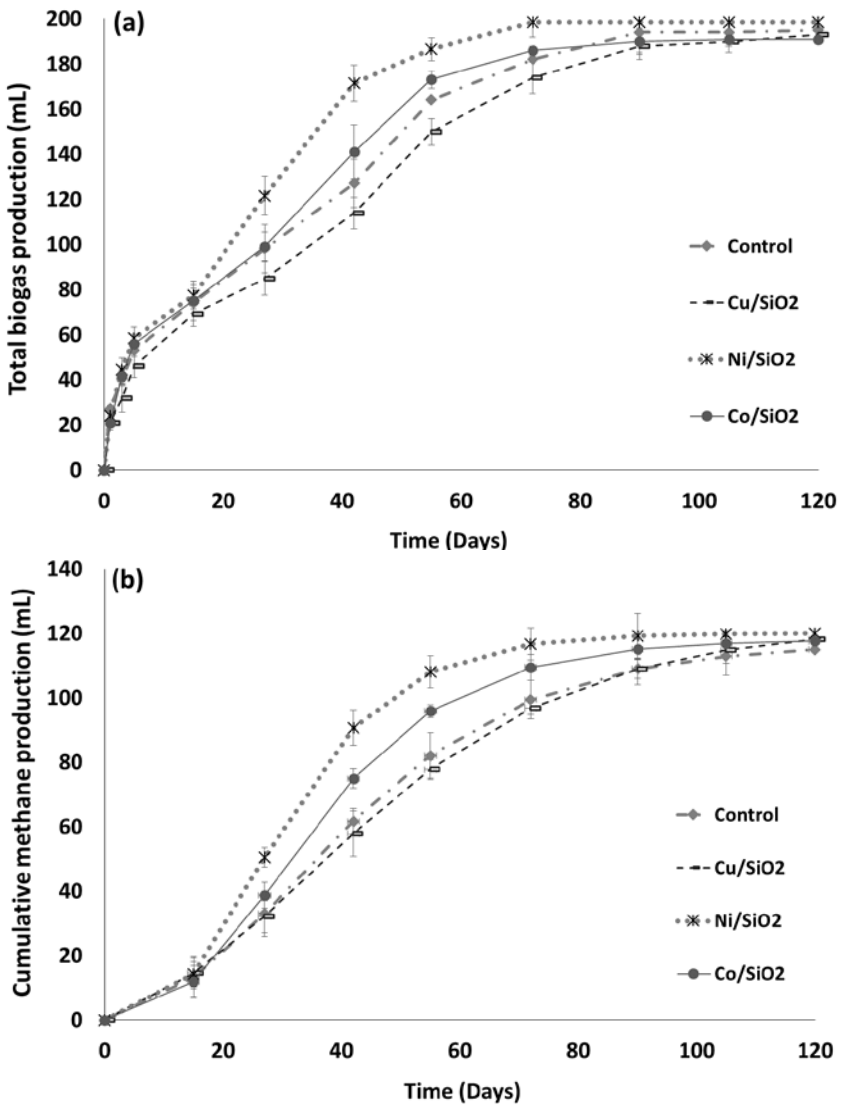

Figure 6. Cumulative volumes of (a) total biogas and (b) methane produced during thermophilic anaerobic digestion of 5 g L^{-1} soluble starch in batch test (serum vials 125 mL) with 10^{-5} mol L^{-1} of encapsulated NPs of Ni/SiO_2, Co/SiO_2 and Cu/SiO_2. The standard deviation bars are calculated based on the triplicate experiments made for each condition.

The maximum methane production rates calculated from the Gompertz model (Table 4) were 70% and 33% higher with Ni/SiO_2 and Co/SiO_2 NPs, respectively, and 11% lower with Cu/SiO_2 NPs than the control without NPs. Again, comprehensively, no significant differences were observed for the maximum cumulative methane productions (mL) at the end of the experiment (i.e., 119.6 ± 2.5 ml), and the calculated lag time ranged between 8.6 and 12.1 days.

The addition of the NPs in the culture batch did not modify the metabolites profile (Figure 7a-d). After one day of incubation, 61–67% of the starch was converted into VFAs and ethanol. Meanwhile, 8%, 12%, 16% and 17% of the starch were converted into lactate, formate, acetate and butyrate, respectively, in the presence of Ni/SiO_2 NPs (Figure 7c), compared with 13%, 11%, 17% and 13% in the presence of Co/SiO_2 NPs (Figure 7d); 27%, 7%, 7% and 16% in the presence of Cu/SiO_2 NPs (Figure 7b); and 11%, 11%, 13% and 20% in the control (Figure 7a). Therefore, copper is associated

with some differences in the general metabolites. The metabolite distribution profiles (Figure 7a-d) showed that the addition of Ni/SiO_2 and Co/SiO_2 NPs, respectively, accelerated the conversion of metabolite into acetate. Then the production of methane that was clear after 15 days of incubation with Ni/SiO_2 NPs (Figure 6). It results a total conversion of metabolites into methane after about 72 days of fermentation (Figure 6).

Table 4. Kinetic parameters and Gompertz coefficient adjusted on the profiles of volumetric methane production curves for the BMP tests with 10^{-5} mol L^{-1} of Ni/SiO_2, Co/SiO_2 and Cu/SiO_2 NPs and 5 g L^{-1} soluble starch.

	λ (days)	μm (mL day^{-1})	A (mL)	R^2
Control	10.2±0.6	1.96±0.13	117.2±2.4	0.9994
Cu/SiO_2	8.6±5	1.74±0.09	122.67±1.8	0.9987
Ni/SiO_2	11.8±9	3.32±0.04	120.20±0.9	0.9995
Co/SiO_2	12.1±3	2.60±0.07	118.12±3.1	0.9997

Standard deviations are calculated based on the triplicate experiments made for each condition.

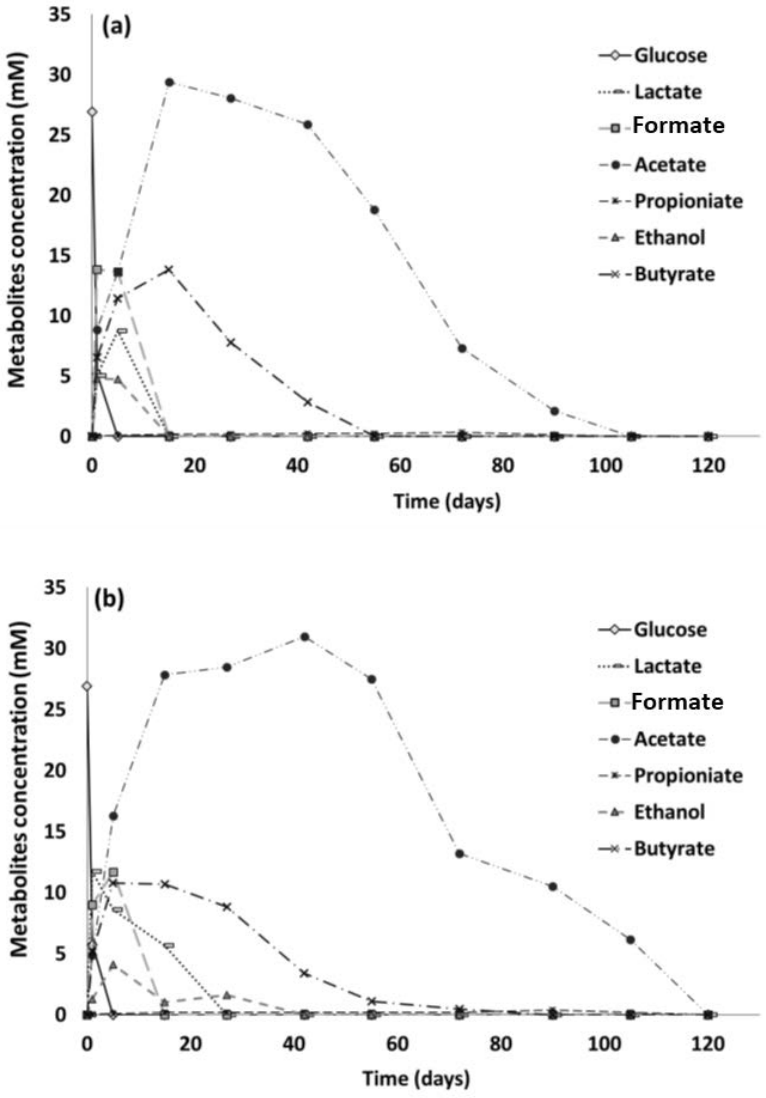

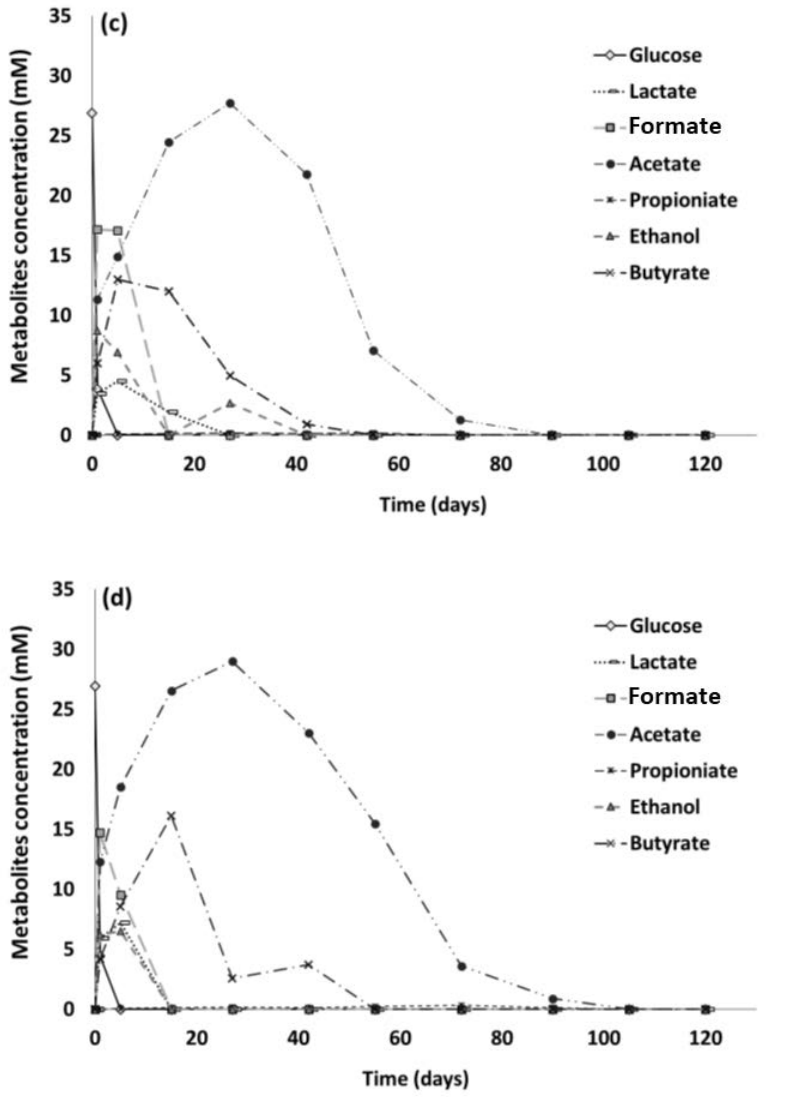

Figure 7. Evolution of metabolic concentrations (mM) during thermophilic anaerobic digestion of 5 g L^{-1} of soluble starch with 10^{-5} mol L^{-1} of encapsulated metal NPs of (b) Cu/SiO_2, (c) Ni/SiO_2 and (d) Co/SiO_2 compared with (a) control without NPs.

3.4. Evaluation of the optimum concentration of nickel NPs on methane production

In a number of serial batch experiments, Ni/SiO_2 NPs at different valence states (i.e, calcined, reduced and dried) and concentrations (10^{-6}, 10^{-5} and 10^{-4} mol L^{-1}) were tested using glucose monohydrate (5 g L^{-1}). The volume of biogas was measured every 15 days during 105 days after the inoculation, with the exception of the first 5 days, where the volume of biogas was measured after 1, 3 and 5 days, since glucose degradation to VFAs is associated with hydrogen production that can lead to inhibition of acetoclastic and hydrogenotrophic methanogens. The results showed that hydrogen production ranged between 40 and 55 mL, with improvement in the presence of calcined Ni/SiO_2 NPs at a concentration of 10^{-4} mol L^{-1} up to 40% above control. Methane production profiles during the incubation period with different Ni/SiO_2 NP concentrations are illustrated in Figures 8a-c. Batch trials with all valence states of Ni/SiO_2 NPs showed higher methane performances than without NPs. After 15 days and whatever the Ni/SiO_2 NP concentration, the methane production was about 15.3 ± 2.0 mL.

During the exponential growth phase, it increased appreciably with increasing Ni/SiO_2 NP concentration up to 10^{-4} mol L^{-1}. At day 60, the methane potential was already produced with the calcined Ni/SiO_2 NPs at a concentration of 10^{-4} mol L^{-1}, whereas 13%, 21% and 25% were still to be produced at concentrations of 10^{-5} and 10^{-6} mol L^{-1} and in the control, respectively. Results were similar with dried Ni/SiO_2 NPs and about 12% lower for reduced Ni/SiO_2 NPs.

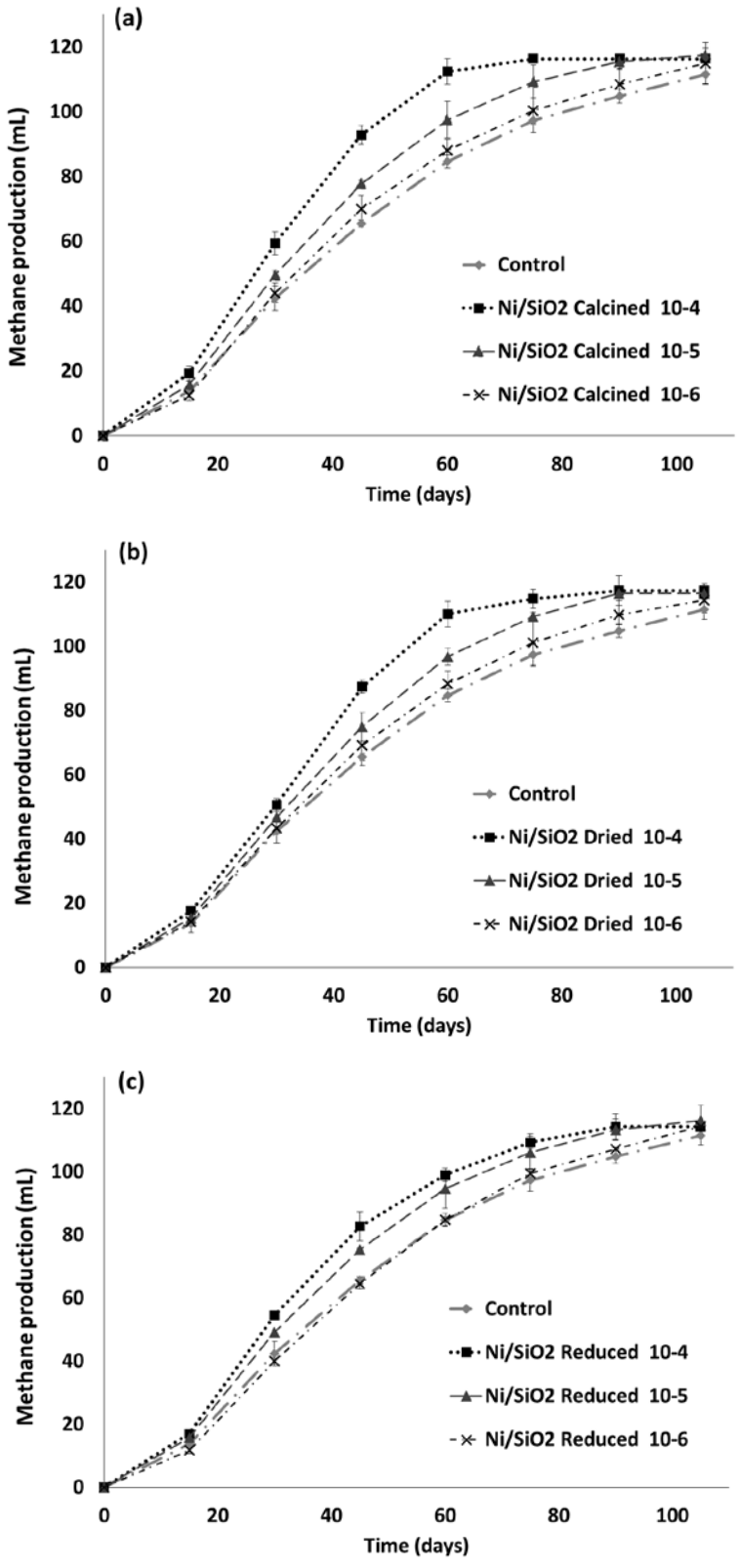

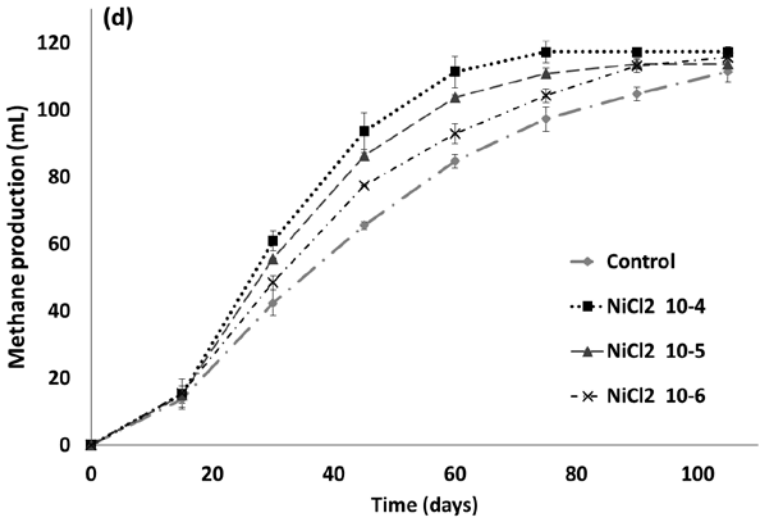

Figure 8. Catalytic effects of different valence states of nickel NPs —(a) calcined Ni/SiO_2 NPs, (b) dried Ni/SiO_2 NPs and (c) reduced Ni/SiO_2 NPs at concentrations of 10^{-6}, 10^{-5} and 10^{-4} mol L^{-1}—on methane production compared with the effect of (d) $NiCl_2$ addition at the same concentrations. The standard deviation bars are calculated based on the triplicate experiments made for each condition.

Batch tests with the addition of $NiCl_2$ were also carried out to compare the influence of different concentrations of $NiCl_2$ with those of Ni/SiO_2 NPs on methane production. The results displayed in Figure 8d confirm the large influence of nickel on methane production and showed that the improvement effect of $NiCl_2$ was higher than that of NPs at 10^{-6} and 10^{-5} mol L^{-1} concentration. Previous studies showed that methane production was enhanced by addition of nickel in concentrations ranging between 10^{-7} and 10^{-4} mol L^{-1} [70–73]. Murray et al. [74] reported that nickel addition (10^{-7} mol L^{-1}) and especially in combination with cobalt and molybdenum increased total biogas and methane production from food processing waste by 42%, while Kumar et al. [75] found that total biogas in anaerobic digestion of potato waste and cattle manure mixture was increased 71% by the addition of nickel (4.26×10^{-5} mol L^{-1}). Work by Qing-Hao Hu et al. [73] has highlighted the possibility of increasing the methane production in anaerobic digestion of synthetic wastewater up to 45% with increasing nickel concentration up to 2×10^{-4} mol L^{-1}. Similar results were obtained by Lo et al. [76], who found that nickel at concentrations varying between 10^{-5} and 10^{-4} mol L^{-1} enhances biogas production.

The results obtained by Gompertz modeling (Table 5) confirm the trends, with the highest maximum methane production (MPR) (3.38 ml/day) achieved with the addition of $NiCl_2$ at a concentration of 10^{-4} mol L^{-1}. The MPR was 86% higher than in the control. Using NPs, the MPR compared to control conditions was higher by 72.1%, 26.3% and 8.5% for calcined Ni/SiO_2 NPs at concentrations of 10^{-4}, 10^{-5} and 10^{-6} mol L^{-1}. Lower effects were achieved with dried and reduced Ni/SiO_2 NPs, varying from 6.3% to 48.6% MPR increases depending on NP concentration (10^{-6} – 10^{-4} mol L^{-1}).

Table 5. Kinetic parameters and Gompertz coefficient adjusted on the profiles of volumetric methane production curves for the BMP tests with different valence states of Ni/SiO_2 NPs and $NiCl_2$ at different concentrations (10^{-6}, 10^{-5} and 10^{-4} mol L^{-1}).

	Metal concentration (mol L^{-1})	λ (days)	μm (mL day^{-1})	A (mL)	R^2
Control	-	8.2±0.5	1.82±0.09	114.2±2.3	0.999
Ni/SiO_2 calcined	10^{-4}	9.9±0.2	3.14±0.14	118.4±0.1	0.999
	10^{-5}	9.1±0.7	2.30±0.01	118.3±3.9	0.999
	10^{-6}	9.1±0.9	1.98±0.04	116.3±4.0	0.999
Ni/SiO_2 dried	10^{-4}	10.6±0.4	2.71±0.15	116.9±2.9	0.999
	10^{-5}	9.4±0.8	2.22±0.16	120.5±0.7	0.999
	10^{-6}	8.6±0.7	1.94±0.23	117.7±3.1	0.999
Ni/SiO_2 reduced	10^{-4}	10.3±0.4	2.46±0.05	120.5±1.7	0.999
	10^{-5}	8.3±0.2	2.15±0.05	118.2±4.7	0.999
	10^{-6}	8.5±0.6	1.99±0.10	115.6±1.1	0.999
$NiCl_2$	10^{-4}	8.3±1.3	3.38±0.21	117.1±0.5	0.999
	10^{-5}	10.4±1.2	2.81±0.13	114.8±1.7	0.999
	10^{-6}	12.4±1.7	2.17±0.27	120.8±3.1	0.999

Standard deviations are calculated based on the triplicate experiments made for each condition.

Regarding metabolites produced from glucose degradation, Figure 10 shows that the main intermediate products during the acidogenic step were lactate, formate, acetate and butyrate. The accumulation of VFA leads to a decrease of medium pH down to the values of 5.2–5.4, which are unfavorable for the methanogens. In the course of the following consumption of VFAs, the medium pH value recovered to 7.2. Lactate, formate and ethanol were the first products converted in acetate (Figure 10b). The BMP tests showed that the presence of Ni/SiO_2 NPs in the medium did not quite modify the metabolites profile but accelerated the consumption of acetate and butyrate by the methanogens and acetogens, respectively. The carbon mass balance calculated on the basis of detected substances at the end of experiment showed that 79±2% of glucose was converted into methane and carbon dioxide for all cases, which was close to results from [77].

3.5. Evaluation of the optimum concentration of Co/SiO_2 NPs on methane production

The improvement effect of different valence states of Co/SiO_2 NPs (i.e., calcined, reduced and dried) using the BMP tests were carried out at different concentrations i.e., 10^{-6}, 10^{-5} and 10^{-4} mol L^{-1}. Experimental conditions were the same used with Ni/SiO_2 NPs. The volume of biogas measured after 1, 3 and 5 days showed a limited effect of cobalt NPs on hydrogen production, while the hydrogen production was 43±4 mL in all conditions. The production of methane profiles during the incubation period from the control and test samples with different concentrations of cobalt NPs are illustrated in Figure 7a–c. No inhibitory effect was observed in all Co/SiO_2 NP treatments. In contrast, the addition of Co/SiO_2 NPs showed consistently positive responses, including increases in methane production. In this experiment, calcined Co/SiO_2 NPs (Figure 9a) showed higher improvement effect on methane production compared with the other forms of Co/SiO_2 NPs, and the results showed that 90% of methane potential was produced in the presence of 10^{-4} mol L^{-1} calcined Co/SiO_2 NPs after 60 days, with increases of 8%, 13% and 14% compared with the concentrations of 10^{-5} and 10^{-4} mol L^{-1} and the

control, respectively. Slightly lesser improvement effects were detected with dried and reduced cobalt NPs. However, cumulative methane yield after 105 days was close for all cases, including the control (i.e., 348 ± 7 mL CH_4 / g glucose), but the presence of Co/SiO_2 NPs accelerated the methane production.

As done with Ni/SiO_2 NPs, batch tests with the addition of $CoCl_2$ were carried out using the same concentrations tested for Co/SiO_2 NPs. Cumulative production of methane during the incubation period from the control and test samples with different concentrations is illustrated in Figure 9 d. The results showed that the stimulatory effect of $CoCl_2$ on methane production was lower at a concentration of 10^{-4} mol L^{-1} by 5% than calcined Co/SiO_2 NPs but still higher by 12% than in the control.

The results obtained by Gompertz modeling (Table 6) showed that cobalt NPs improved MPR by 44.9, 18.4 and 7.1%, respectively, compared to the control, via calcined Co/SiO_2 NPs at concentrations of 10^{-4}, 10^{-5} and 10^{-6} mol L^{-1}. Lower improvement effects were observed with dried and reduced cobalt NPs, with MPR increases varying between 2.7% and 17.6%, depending on NP concentration (10^{-6}–10^{-4} mol L^{-1}). Meanwhile, the addition of $CoCl_2$ increased the MPR up to 30.2% with a concentration of 10^{-4} mol L^{-1}.

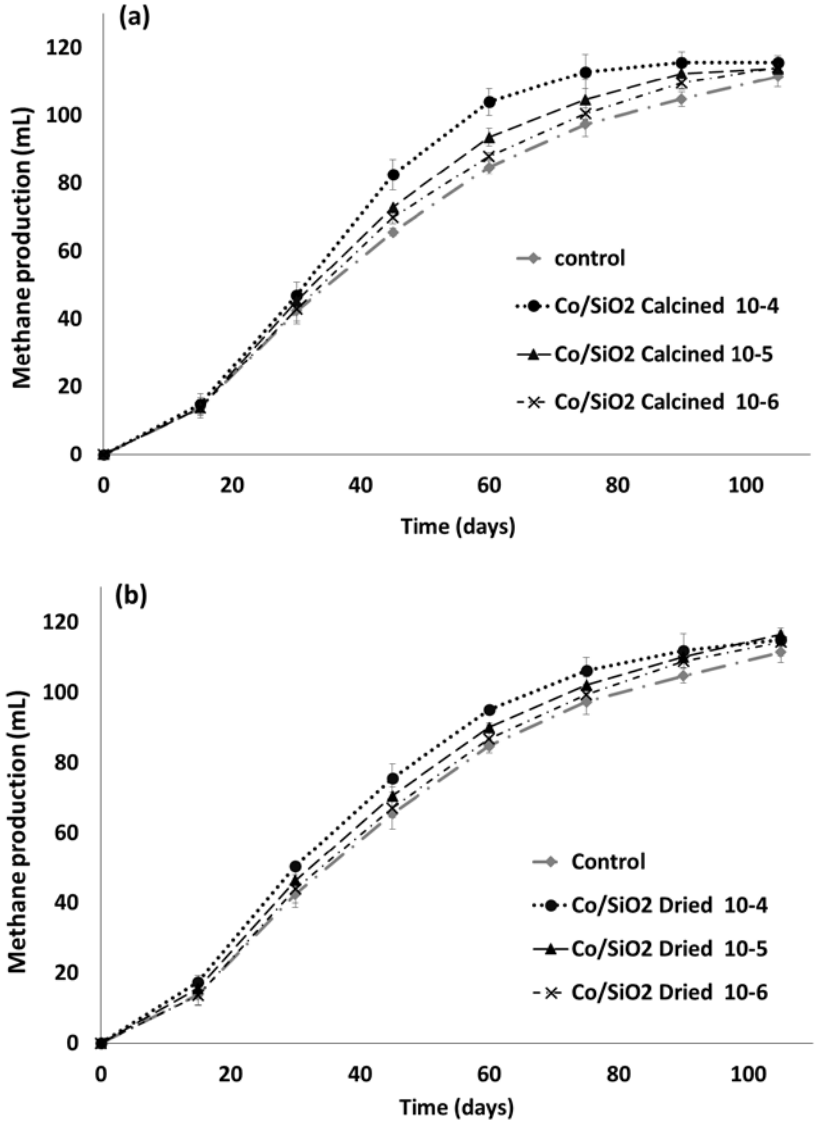

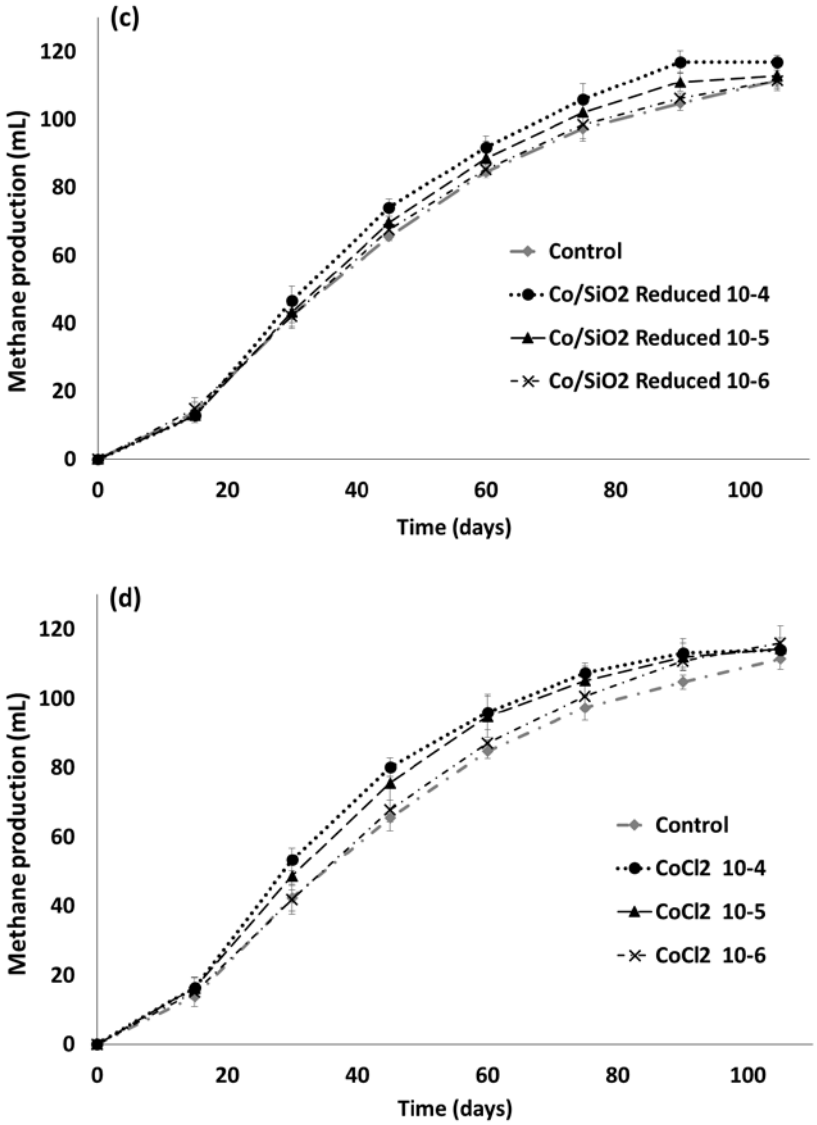

Figure 9. Catalytic effects of different valence states of cobalt NPs—(a) calcined Co/SiO_2 NPs, (b) dried Co/SiO_2 NPs and (c) reduced Co/SiO_2 NPs at concentrations of 10^{-6}, 10^{-5} and 10^{-4} mol L^{-1}—on methane production, compared with the effect of (d) $CoCl_2$ addition at the same concentrations. The standard deviation bars are calculated based on the triplicate experiments made for each condition.

Table 6. Kinetic parameters and Gompertz coefficient adjusted on the profiles of volumetric methane production curves for the BMP tests with different valence states of Co/SIO_2 NPs and $CoCl_2$ at different concentrations (10^{-6}, 10^{-5} and 10^{-4} mol L^{-1}).

	Metal concentration (mol L^{-1})	λ (days)	μm (mL day^{-1})	A (mL)	R^2
Control	-	8.2±0.5	1.82±0.09	114.2±2.3	0.9997
	10^{-4}	11.6±1.2	2.64±0.23	118.5±1.4	0.9996
Co/SiO_2 calcined	10^{-5}	9.8±0.8	2.16±0.20	116.9±0.4	0.9992
	10^{-6}	8.9±1.9	1.96±0.18	117.2±3.3	0.9993
	10^{-4}	7.5±1.4	2.14±0.04	115.7±1.4	0.9993
Co/SiO_2 dried	10^{-5}	7.5±0.3	1.94±0.04	117.1±0.1	0.9992
	10^{-6}	8.2±0.4	1.87±0.20	116.9±4.3	0.9995
	10^{-4}	9.4±1.7	2.12±0.05	120.2±0.7	0.9993
Co/SiO_2 reduced	10^{-5}	9.5±1.1	2.01±0.12	116.7±1.3	0.9992
	10^{-6}	8.1±0.1	1.85±0.05	115.2±1.0	0.9997
	10^{-4}	8.3±1.0	2.37±0.29	116.7±0.9	0.9993
$CoCl_2$	10^{-5}	8.3±0.7	2.17±0.04	116.3±3.3	0.9992
	10^{-6}	8.2±0.1	1.86±0.06	117.8±2.5	0.9991

Standard deviations are calculated on the triplicates experiments made for each condition.

As shown in Figure 10, the most obvious difference in metabolite changes between the control without NPs and Co/SiO_2 NPs was that the addition of 10^{-4} mol L^{-1} calcined cobalt NPs increased the conversion of fatty acids to acetate (Figure 10c). The results showed that Co/SiO_2 NPs accelerate the consumption of acetate to produce methane compared with the control without NPs (Figure 10a), which was clear after 30 days of fermentation.

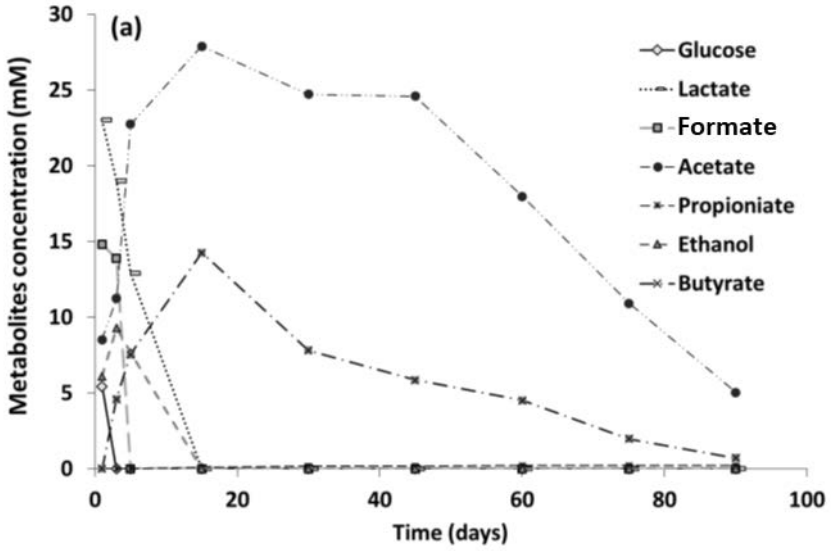

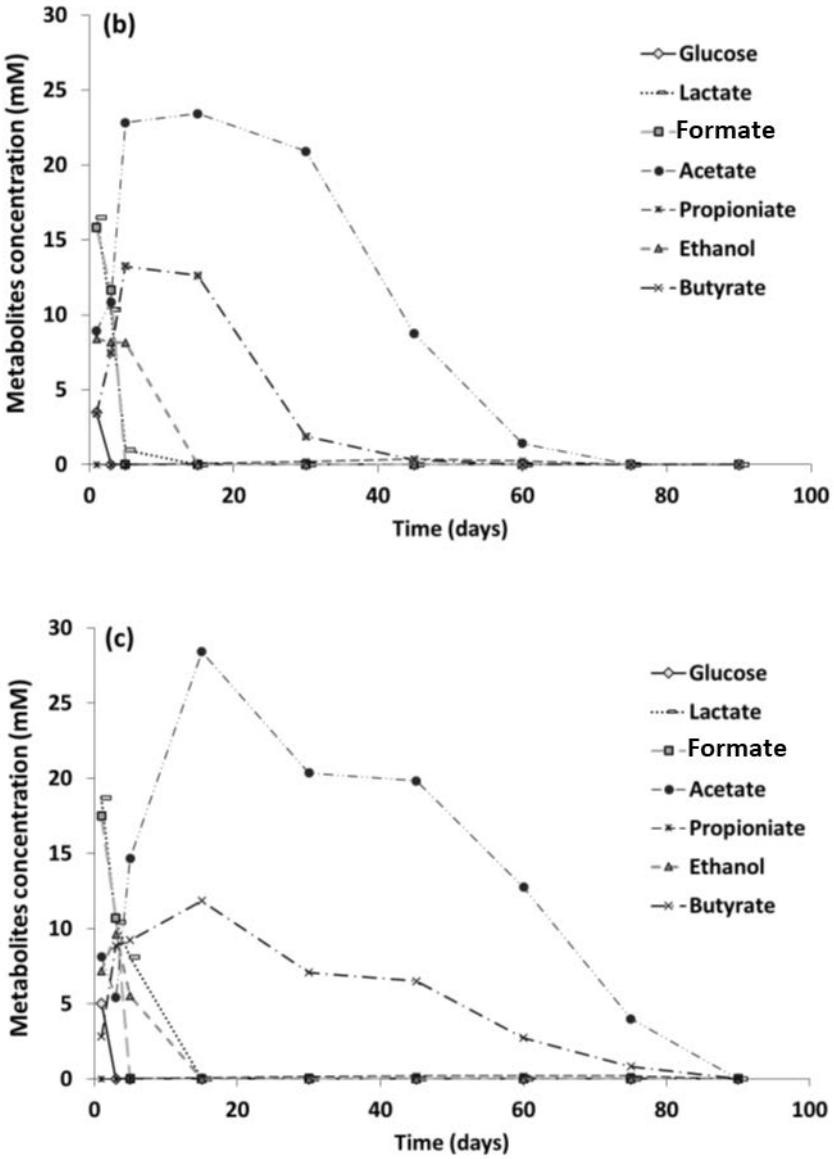

Figure 10. The changes of metabolic concentration (mM) during thermophilic anaerobic digestion of 5 g L^{-1} of glucose monohydrate with 10^{-4} mol L^{-1} of (b) calcined Ni/SiO_2 and (c) calcined Co/SiO_2 NPs compared with (a) control without NPs.

4. Discussion

The presence of heavy metal ions (i.e., Cu, Zn, Fe, Ni, Co, Mo) during anaerobic biodegradation of organic matter is known to be fundamental for numerous reactions. The present studies on anaerobic digestion with different metal NP additives showed that methane production was affected by different metal NPs and by NP concentration. Nickel addition had a clear stimulating effect on the methane production from all tested substrates. This can be explained by the fact that nickel is an essential cofactor for a number of enzymatic reactions, and nickel-containing enzymes are involved in at least five metabolic processes, including methanogenesis [78]. Ragsdale [79] reported that nickel can exist in oxidation states from 0 to $^{+}4$ in biology, and the nickel redox enzymes appear to access either the $2^{+}/1^{+}$ and/or the $3^{+}/2^{+}$ redox couples. In addition, the zero-valence state is important during catalysis by acetyl-CoA synthase, and the hydrolases appear to only use Ni^{2+}, which is a Lewis acid. However,

our results showed uneven positive effects of Ni/SiO_2 and Co/SiO_2 NPs at different oxidation states.

The effects of NPs on anaerobic digestion were studied by many authors [25,26,80,81]. Most studies focus on the antimicrobial function of NPs on methanogenic activities, which is related to the liberation of metal ions. Studies of catalytic effect of NPs on anaerobic digestion are limited to enhancement of fermentative bio-hydrogen production [28,32], and mechanisms of the NP effects are not clear. Qilin et al. [82] suggested that NPs can be sorbed onto cell surfaces and thereby alter the membrane properties (e.g., increase membrane permeability,) which leads to more efficient electron transfer to an acceptor. Beckers et al. [32] suggested that NPs played a role of active catalytic site involved in the production of hydrogen and are used by the bacteria for oxidation/reduction chemical reaction to help the bacteria transfer its electrons faster without consuming or metabolizing the metal, as when it is added to the medium in a dissolved form. An investigation was carried out in our lab on iron NPs at concentrations varying between 10^{-4} and 10^{-3} M using ICP-AES (inductively coupled plasma atomic emission spectrometry), which showed that 10^{-7} M of iron ions were released from autoclaved iron NPs, and this concentration increased with time. The advantage of using metal NPs in anaerobic bio-methane production is that the NPs are encapsulated inside the porous silica matrix, which limits the metal ions' liberation in the culture medium. Thus, bacteria can uptake metals gradually, attaining sufficiently high intracellular metal concentrations to meet the demand of the metal enzymes and avoiding toxicity or other problems commonly associated with higher concentration of metals in bacteria and also metal precipitation. This secures the bacteria's need of metal for a longer time compared with the addition of other forms of metal, in addition to the extracellular role that may be played by NPs as active catalytic sites, as mentioned by [32].

In Table 7, the present study is compared to the literature by summarizing the most important parameters and results of each study concerning the production of bio-methane using metallic NP materials as catalysts.

It can be observed directly that making a comparison is quite difficult because many conditions such as the type of NPs, their concentration or the substrate differ greatly from one study to another. Nevertheless, it is observed that the Ni NPs are materials that lead to high methane production in this present study but also in Gran et al. [30] and Abdelsalam et al. [83]. In Zhang et al. [16], the Fe NPs are also encapsulated in a matrix but in chitosan, compared to porous silica used in this present study. It is also observed that not much information about the NPs is given, such as electron microscope image or specific surface area.

Table 7. Literature comparison of methane production in anaerobic digestion catalyzed by metallic NPs.

Reference	NPs type	Conditions	Results on methane production
The present study	Cu/SiO_2, Pd/SiO_2, Pt/SiO_2, Ni/SiO_2, Co/SiO_2, Ag/SiO_2 and Fe/SiO_2	Acetate, starch or glucose substrate Between 10^{-6} and 10^{-4} mol/L	+ 72% of methane production compared to control with the best sample (Ni)
Bakari et al. 2023 [18]	Fe^0 form steel wool or steel craps	Sludge substrate NPs concentration of 10 g/L	+ 12% of methane production compared to control with the best sample
Gran et al. 2022 [30]	NiO, CoO, and Fe_3O_4	Sludge substrate NPs concentration of 1, 10 or 100 mg/L	+ 62,65% of methane production compared to control with the best sample
Zhang et al. 2024 [16]	Fe(III)/Chitosan	Sludge substrate NPs concentration of 5, 10 or 20 g/L	+ 23% of methane production compared to control with the best sample
Abdelsalam et al. 2016 [83]	Co (30 nm), Ni (20 nm), Fe (10 nm), Fe_3O_4 (10 nm)	Fresh raw manure substrate NPs concentration of 1, 2 or 20 mg/L	+ 116% of methane production compared to control with the best sample (Ni)
Grosser et al. 2021 [84]	$AgNO_3$ or Ag NPs	Sewage sludge substrate NPs concentration of 40 mg/L	+ 25% of methane production compared to control with the best sample

5. Conclusions

In this work, seven types of encapsulated metal NPs were used as potential catalysts in thermophilic anaerobic digestion to produce methane. These NPs were produced thanks to a sol-gel method called cogelification. This process allows the dispersion of metallic NPs in a highly porous silica matrix, allowing a constant release of metal in water medium and avoiding the agglomeration of the NPs. All seven NPs showed this typical morphology.

Then, the seven metal NPs (Cu/SiO_2, Pd/SiO_2, Pt/SiO_2, Ni/SiO_2, Co/SiO_2, Ag/SiO_2 and Fe/SiO_2) were used and compared for bio-methane production from acetate substrate. The cumulative methane production and production rate were investigated and modeled according to the Gompertz equation to identify the best catalysts. It was found that only Ni/SiO_2, Co/SiO_2 and Cu/SiO_2 showed stimulatory effects on methane generation from acetate.

In the last part of this work, the two best catalysts, Ni/SiO_2 and Co/SiO_2, were used for bio-methane production with two other carbon substrates: starch and glucose. The effects of NP concentration and the type of thermal pre-treatment of NPs on the methane production were

investigated. The result was that the methane production was higher with Ni/SiO_2 NPs. In addition, it was found that calcined NPs were the most efficient, almost evenly with dried ones. Similar profiles of intermediate fermentation products were recorded between Ni- and Co/SiO_2 catalysts. The influence of those NPs on methane production rate was concentration dependent, increasing with the increase of metal NPs concentration from 10^{-6} to 10^{-4} mol L^{-1}. Finally, with the best catalyst, Ni/SiO_2, a production of bio-methane 72.1% higher than the control was obtained.

Acknowledgments

This work was financially supported by a grant from the AECS –Syria, and we also thank the Centre Wallon de Biologie Industrielle-CWBI (Liege, Belgium) for support.
Julien G. Mahy and Stéphanie D. Lambert thank the F.R.S.-FNRS for their Postdoctoral Researcher position and Research Director position, respectively. J.G.M. is grateful to the Rotary for a District 2160 grant, to the University of Liège and the FNRS for financial support for a postdoctoral stay at INRS Centre Eau, Terre, Environnement in Québec, Canada.

Author contributions

Alaa E. Al-Ahmad: conceptualization, methodology, writing – original draft, writing – review & editing, investigation, formal analysis. Stéphanie D. Lambert: conceptualization, methodology, writing – review & editing, funding acquisition. Julien G. Mahy: investigation, formal analysis, writing – review & editing. Benoît Heinrichs: investigation, formal analysis. Wissal Wannoussa: investigation, formal analysis. Ludivine Tasseroul: investigation, formal analysis. Frédéric Weekers: investigation, formal analysis. Philippe Thonart: supervision, funding acquisition, project administration. Serge Hiligsmann: conceptualization, methodology, writing – original draft, writing – review & editing, investigation, formal analysis, supervision, funding acquisition, project administration.

Data availability statement

The raw/processed data required to reproduce these findings can be shared on demand.

Conflict of interest

The authors declare that there is no conflict of interest concerning this work.

References

1. Ter Heijne A, Hamelers HVM, Buisman CJN (2007) Microbial fuel cell operation with continuous biological ferrous iron oxidation of the catholyte. *Environ Sci Technol* 41: 4130–4134. https://doi.org/10.1021/es0702824
2. Alkan-Ozkaynak A, Karthikeyan KG (2011) Anaerobic digestion of thin stillage for energy recovery and water reuse in corn-ethanol plants. *Bioresour Technol* 102: 9891–9896. https://doi.org/10.1016/j.biortech.2011.08.028

3. Rocha-Meneses L, Hari A, Inayat A, et al (2022) Application of nanomaterials in anaerobic digestion processes: A new strategy towards sustainable methane production. *Biochem Eng J* 188: 108694. https://doi.org/10.1016/j.bej.2022.108694
4. Weiland P (2010) Biogas production: Current state and perspectives. *Appl Microbiol Biotechnol* 85:849–860. https://doi.org/10.1007/s00253-009-2246-7
5. Zheng X, Zou D, Wu Q, et al (2022) Review on fate and bioavailability of heavy metals during anaerobic digestion and composting of animal manure. *Waste Management* 150: 75–89. https://doi.org/10.1016/j.wasman.2022.06.033
6. Zhao W, Zheng Y-M, Shuai, et al (2009) Effect of Hexavalent Chromium on Performance of Membrane Bioreactor in Wastewater Treatment. *J Environ Engin* 135: 796–805. https://doi.org/10.1061/ASCE0733-93722009135:9796
7. Lee YJ, Lee DJ (2019) Impact of adding metal nanoparticles on anaerobic digestion performance – A review. *Bioresour Technol* 292: 121926. https://doi.org/10.1016/j.biortech.2019.121926
8. Pobeheim H, Munk B, Johansson J, Guebitz GM (2010) Influence of trace elements on methane formation from a synthetic model substrate for maize silage. *Bioresour Technol* 101: 836–839. https://doi.org/10.1016/j.biortech.2009.08.076
9. Hausinger RP (1987) Nickel Utilization by Microorganisms. *Microbiol Rev* 51: 22–42
10. Diekert G, Konheiser U, Piechulla K, Mikrobiologie RKT (1981) Nickel Requirement and Factor F430 Content of Methanogenic Bacteria. *J Bacteriol* 148: 459–464
11. Banks CJ, Zhang Y, Jiang Y, Heaven S (2012) Trace element requirements for stable food waste digestion at elevated ammonia concentrations. *Bioresour Technol* 104: 127–135. https://doi.org/10.1016/j.biortech.2011.10.068
12. Hassanein A, Naresh Kumar A, Lansing S (2021) Impact of electro-conductive nanoparticles additives on anaerobic digestion performance - A review. *Bioresour Technol* 342: 126023. https://doi.org/10.1016/j.biortech.2021.126023
13. Feng XM, Karlsson A, Svensson BH, Bertilsson S (2010) Impact of trace element addition on biogas production from food industrial waste - Linking process to microbial communities. *FEMS Microbiol Ecol* 74: 226–240. https://doi.org/10.1111/j.1574-6941.2010.00932.x
14. Zhu X, Blanco E, Bhatti M, Borrion A (2021) Impact of metallic nanoparticles on anaerobic digestion: A systematic review. *Sci Total Environ* 757: 143747. https://doi.org/10.1016/j.scitotenv.2020.143747
15. Patel GB (1984) Characterization and nutritional properties of Methanothrix concilii sp. nov., a mesophilic, aceticlastic methanogen. *Can J Microbiol* 30: 1383-1396.
16. Zhang B, Zhao Z, Ma R, et al (2024) Unveiling the mechanisms of Fe (III)-loaded chitosan composite (CTS-Fe) in enhancing anaerobic digestion of waste activated sludge. *J Environ Sci* (China) 138: 200–211. https://doi.org/10.1016/j.jes.2023.04.001
17. Jadhava P, Muhammad N, Bhuyar P, et al (2021) A review on the impact of conductive nanoparticles (CNPs) in anaerobic digestion: Applications and limitations. *Environ Technol Innov* 23: 101526. https://doi.org/10.1016/j.eti.2021.101526
18. Bakari O, Njau KN, Noubactep C (2023) Effects of zero-valent iron on sludge and methane production in anaerobic digestion of domestic wastewater. *Case Stud Chemical Environ Engin* 8: 100377. https://doi.org/10.1016/j.cscee.2023.100377
19. Schonheit P, Moll J, Thauer RK (1979) Nickel, Cobalt, and Molybdenum Requirement for Growth of Methanobacterium thermoautotrophicum. *Arch Microbiol* 123: 105–107

20. Zandvoort MH, van Hullebusch ED, Fermoso FG, Lens PNL (2006) Trace metals in anaerobic granular sludge reactors: Bioavailability and dosing strategies. *Eng Life Sci* 6: 293–301. https://doi.org/10.1002/elsc.200620129
21. Ehrlich HL (2002) Geomicrobiology. M. Dekker
22. Králik M, Biffis A (2001) Catalysis by metal nanoparticles supported on functional organic polymers. *J Mol Catal A Chem* 177: 113–138
23. Sergeev GB (2003) Cryochemistry of metal nanoparticles. *J Nanopart Res* 5: 529–537
24. Barrena R, Moral-Vico J, Font X, Sánchez A (2022) Enhancement of Anaerobic Digestion with Nanomaterials: A Mini Review. *Energies (Basel)* 15: 5087. https://doi.org/10.3390/en15145087
25. Gonzalez-Estrella J, Sierra-Alvarez R, Field JA (2013) Toxicity assessment of inorganic nanoparticles to acetoclastic and hydrogenotrophic methanogenic activity in anaerobic granular sludge. *J Hazard Mater* 260: 278–285. https://doi.org/10.1016/j.jhazmat.2013.05.029
26. Mu H, Chen Y, Xiao N (2011) Effects of metal oxide nanoparticles (TiO2, Al2O3, SiO2 and ZnO) on waste activated sludge anaerobic digestion. *Bioresour Technol* 102: 10305–10311. https://doi.org/10.1016/j.biortech.2011.08.100
27. Luna-delRisco M, Orupõld K, Dubourguier HC (2011) Particle-size effect of CuO and ZnO on biogas and methane production during anaerobic digestion. *J Hazard Mater* 189: 603–608. https://doi.org/10.1016/j.jhazmat.2011.02.085
28. Zhao W, Zhang Y, Du B, et al (2013) Enhancement effect of silver nanoparticles on fermentative biohydrogen production using mixed bacteria. *Bioresour Technol* 142: 240–245. https://doi.org/10.1016/j.biortech.2013.05.042
29. Han H, Cui M, Wei L, et al (2011) Enhancement effect of hematite nanoparticles on fermentative hydrogen production. *Bioresour Technol* 102: 7903–7909. https://doi.org/10.1016/j.biortech.2011.05.089
30. Gran S, Motiee H, Mehrdadi N, Tizghadam M (2022) Impact of Metal Oxide Nanoparticles (NiO, CoO and Fe3O4) on the Anaerobic Digestion of Sewage Sludge. *Waste Biomass Valori* 13: 4549–4563. https://doi.org/10.1007/s12649-022-01816-8
31. Zhang Y, Shen J (2007) Enhancement effect of gold nanoparticles on biohydrogen production from artificial wastewater. *Int J Hydrogen Energy* 32: 17–23. https://doi.org/10.1016/j.ijhydene.2006.06.004
32. Beckers L, Hiligsmann S, Lambert SD, et al (2013) Improving effect of metal and oxide nanoparticles encapsulated in porous silica on fermentative biohydrogen production by Clostridium butyricum. *Bioresour Technol* 133: 109–117. https://doi.org/10.1016/j.biortech.2012.12.168
33. Jiao J, Wan J, Ma Y, Wang Y (2019) Enhanced photocatalytic activity of AgNPs-in-CNTs with hydrogen peroxide under visible light irradiation. *Environmental Science and Pollution Research* 26: 26389–26396. https://doi.org/10.1007/s11356-019-05877-6
34. Majles Ara MH, Dehghani Z, Sahraei R, Nabiyouni G (2010) Non-linear optical properties of silver nanoparticles prepared by hydrogen reduction method. *Opt Commun* 283: 1650–1653. https://doi.org/10.1016/j.optcom.2009.09.025
35. Bulavinets T, Varyshchuk V, Yaremchuk I, Bobitski Y (2018) Design and synthesis of silver nanoparticles with different shapes under the influence of photon flows. In: Springer Proceedings in Physics. Springer Science and Business Media, LLC, pp 231–241.

36. Koohpeima F, Mokhtari MJ, Khalafi S (2017) The effect of silver nanoparticles on composite shear bond strength to dentin with different adhesion protocols. *J Appl Oral Sci* 25: 367–373. https://doi.org/10.1590/1678-7757-2016-0391
37. Song H, Zhang H, Sun Z, et al (2019) Triangular silver nanoparticle U-bent fiber sensor based on localized surface plasmon resonance. *AIP Adv* 9. https://doi.org/10.1063/1.5111820
38. Van Cleve T, Gibara E, Linic S (2016) Electrochemical Oxygen Reduction Reaction on Ag Nanoparticles of Different Shapes. *ChemCatChem* 8: 256–261
39. Saeed W, Abbasi Z, Bilal M, et al (2023) Interactive behavior of graphene quantum dots towards noble metal surfaces. *Physica E Low Dimens Syst Nanostruct* 147: 115596. https://doi.org/10.1016/j.physe.2022.115596
40. Zhang Y, Yang Z, Zou Y, et al (2023) Novel Ag-coated nanofibers prepared by electrospraying as a SERS platform for ultrasensitive and selective detection of nitrite in food. *Food Chem* 135563. https://doi.org/10.1016/j.foodchem.2023.135563
41. Truong TK, Nguyen TQ, Phuong La HP, et al (2021) Insight into the degradation of p-nitrophenol by visible-light-induced activation of peroxymonosulfate over Ag/ZnO heterojunction. *Chemosphere* 268: 129291. https://doi.org/10.1016/j.chemosphere.2020.129291
42. Wasilewska A, Klekotka U, Zambrzycka M, et al (2023) Physico-chemical properties and antimicrobial activity of silver nanoparticles fabricated by green synthesis. *Food Chem* 400: 133960. https://doi.org/10.1016/j.foodchem.2022.133960
43. Dhanya NP (2017) Non linear optical investigations of silver nanoparticles synthesised by curcumin reduction. *Opt Mater (Amst)* 73: 384–387. https://doi.org/10.1016/j.optmat.2017.08.026
44. Mahy JG, Claude V, Sacco L, Lambert SD (2017) Ethylene polymerization and hydrodechlorination of 1,2-dichloroethane mediated by nickel(II) covalently anchored to silica xerogels. *J Solgel Sci Technol* 81: 59–68. https://doi.org/10.1007/s10971-016-4272-0
45. Claude V, Mahy JG, Douven S, et al (2019) Ni- and Fe-doped g-Al2O3 or olivine as primary catalyst for toluene reforming. *Mater Today Chem* 14: 100197. https://doi.org/10.1016/j.mtchem.2019.100197
46. Douven S, Mahy JG, Wolfs C, et al (2020) Efficient N, Fe Co-doped TiO2 active under cost-effective visible LED light: From powders to films. *Catalysts* 10: 547. https://doi.org/10.3390/catal10050547
47. Abou Elez RMM, Attia ASA, Tolba HMN, et al (2023) Molecular identification and antiprotozoal activity of silver nanoparticles on viability of Cryptosporidium parvum isolated from pigeons, pigeon fanciers and water. *Sci Rep* 13: 3109. https://doi.org/10.1038/s41598-023-30270-2
48. Manikandan DB, Sridhar A, Krishnasamy Sekar R, et al (2021) Green fabrication, characterization of silver nanoparticles using aqueous leaf extract of Ocimum americanum (Hoary Basil) and investigation of its in vitro antibacterial, antioxidant, anticancer and photocatalytic reduction. *J Environ Chem Eng* 9: 104845. https://doi.org/10.1016/j.jece.2020.104845
49. Rahman AU, Khan AU, Yuan Q, et al (2019) Tuber extract of Arisaema flavum eco-benignly and effectively synthesize silver nanoparticles: Photocatalytic and antibacterial response against multidrug resistant engineered E. coli QH4. *J Photochem Photobiol B* 193: 31–38. https://doi.org/10.1016/j.jphotobiol.2019.01.018

50. Samuel MS, Jose S, Selvarajan E, et al (2020) Biosynthesized silver nanoparticles using Bacillus amyloliquefaciens; Application for cytotoxicity effect on A549 cell line and photocatalytic degradation of p-nitrophenol. *J Photochem Photobiol B* 202: 111642. https://doi.org/10.1016/j.jphotobiol.2019.111642
51. Mahy JG, Tasseroul L, Zubiaur A, et al (2014) Highly dispersed iron xerogel catalysts for p-nitrophenol degradation by photo-Fenton effects. *Microporous and Mesoporous Materials* 197: 164–173. https://doi.org/10.1016/j.micromeso.2014.06.009
52. Mahy JG, Tasseroul L, Tromme O, et al (2019) Hydrodechlorination and complete degradation of chlorinated compounds with the coupled action of Pd/SiO<inf>2</inf> and Fe/SiO<inf>2</inf> catalysts: Towards industrial catalyst synthesis conditions. *J Environ Chem Eng* 7: 103014. https://doi.org/10.1016/j.jece.2019.103014
53. Mahy JG, Delbeuck T, Tran KY, et al (2023) Green Chemistry for the Transformation of Chlorinated Wastes: Catalytic *Hydrodechlorination on Pd-Ni and Pd-Fe Bimetallic Catalysts Supported on SiO2*. *Gels* 9: 275. https://doi.org/10.3390/gels9040275
54. Lambert S, Alié C, Pirard JP, Heinrichs B (2004) Study of textural properties and nucleation phenomenon in Pd/SiO2, Ag/SiO2 and Cu/SiO2 cogelled xerogel catalysts. *J Non Cryst Solids* 342: 70–81. https://doi.org/10.1016/j.jnoncrysol.2004.06.005
55. Heinrichs B, Rebbouh L, Geus JW, et al (2008) Iron(III) species dispersed in porous silica through sol-gel chemistry. *J Non Cryst Solids* 354: 665–672. https://doi.org/10.1016/j.jnoncrysol.2007.07.071
56. Mahy JG, Lambert SD, Léonard GLM, et al (2016) Towards a large scale aqueous sol-gel synthesis of doped TiO2: Study of various metallic dopings for the photocatalytic degradation of p-nitrophenol. *J Photochem Photobiol A Chem* 329: 189–202. https://doi.org/10.1016/j.jphotochem.2016.06.029
57. Hiligsmann S, Masset J, Hamilton C, et al (2011) Comparative study of biological hydrogen production by pure strains and consortia of facultative and strict anaerobic bacteria. *Bioresour Technol* 102: 3810–3818. https://doi.org/10.1016/j.biortech.2010.11.094
58. Hamilton C, Hiligsmann S, Beckers L, et al (2010) Optimization of culture conditions for biological hydrogen production by Citrobacter freundii CWBI952 in batch, sequenced-batch and semicontinuous operating mode. *Int J Hydrogen Energy* 35: 1089–1098. https://doi.org/10.1016/j.ijhydene.2009.10.073
59. Gil MM, Brandão TRS, Silva CLM (2006) A modified Gompertz model to predict microbial inactivation under time-varying temperature conditions. *J Food Eng* 76: 89–94. https://doi.org/10.1016/j.jfoodeng.2005.05.017
60. Zwietering MH, Jongenburger I, Rombouts FM, et al (1990) Modeling of the Bacterial Growth Curve. *Appl Environ Microbiol* 1875–1881
61. Zhu B, Gikas P, Zhang R, et al (2009) Characteristics and biogas production potential of municipal solid wastes pretreated with a rotary drum reactor. *Bioresour Technol* 100: 1122–1129. https://doi.org/10.1016/j.biortech.2008.08.024
62. Lambert S, Cellier C, Grange P, et al (2004) Synthesis of Pd/SiO2, Ag/SiO2, and Cu/SiO2 cogelled xerogel catalysts: Study of metal dispersion and catalytic activity. *J Catal* 221: 335–346. https://doi.org/10.1016/j.jcat.2003.07.014
63. Toshima N (2004) METAL NANOPARTICLES FOR CATALYSIS. In: Liz-Marzán L, Kamat P (eds) Nanoscale Materials. Springer, pp 79–96

64. Hickey RF, Vanderwielen J, Switzenbaum MS (1989) THE EFFECT OF HEAVY METALS ON METHANE PRODUCTION AND HYDROGEN AND CARBON MONOXIDE LEVELS DURING BATCH ANAEROBIC SLUDGE DIGESTION. *Water Res* 23: 207–218
65. Sasaki K, Morita M, Hirano S ichi, et al (2009) Effect of adding carbon fiber textiles to methanogenic bioreactors used to treat an artificial garbage slurry. *J Biosci Bioeng* 108: 130–135. https://doi.org/10.1016/j.jbiosc.2009.03.003
66. Fathepure BZ (1987) Factors Affecting the Methanogenic Activity of Methanothrix soehngenii VNBFt. *Appl Environ Microbiol* 53: 2978–2982
67. Wu D, Yang Z, Tian G (2011) Inhibitory effects of Cu (II) on fermentative methane production using bamboo wastewater as substrate. *J Hazard Mater* 195: 170–174. https://doi.org/10.1016/j.jhazmat.2011.08.021
68. Karri S, Sierra-Alvarez R, Field JA (2006) Toxicity of copper to acetoclastic and hydrogenotrophic activities of methanogens and sulfate reducers in anaerobic sludge. *Chemosphere* 62: 121–127. https://doi.org/10.1016/j.chemosphere.2005.04.016
69. Pavlostathis SG, Maeng SK (2000) FATE AND EFFECT OF SILVER ON THE ANAEROBIC DIGESTION PROCESS. *Water Res* 34: 3957–3966
70. Williams CM, Shih JCH, Spears JW (1986) Effect of Nickel on Biological Methane Generation from a Laboratory Poultry Waste Digester. *Biotechnol Bioeng* 28: 1608–1610
71. Canovas-Diaz M, Howell JA (1986) EFFECT OF NICKEL ON METHANE PRODUCTION AND BUTYRIC ACID UTILIZATION IN A DOWNFLOW FIXED-FILM REACTOR. *Biotechnol Lett* 8: 287–292
72. Gonzalez-Gil G, Kleerebezem R, Lettinga G (1999) Effects of Nickel and Cobalt on Kinetics of Methanol Conversion by Methanogenic Sludge as Assessed by On-Line CH 4 Monitoring. *Appl Environ Microbiol* 65: 1789–1793
73. Hu QH, Li XF, Liu H, et al (2008) Enhancement of methane fermentation in the presence of Ni2+ chelators. *Biochem Eng J* 38: 98–104. https://doi.org/10.1016/j.bej.2007.07.002
74. Murray WD, Van Den Berg L (1981) Effects of Nickel, Cobalt, and Molybdenum on Performance of Methanogenic Fixed-Film Reactorst. *Appl Environ Microbiol* 42: 502–505
75. Kumar A, Miglani P, Gupta RK, Bhattacharya TK (2006) Impact of Ni(II), Zn(II) and Cd(II) on biogassification of potato waste. *J Environ Biol* 27: 61–66
76. Lo HM, Chiang CF, Tsao HC, et al (2012) Effects of spiked metals on the MSW anaerobic digestion. *Waste Manage Res* 30: 32–48. https://doi.org/10.1177/0734242X10383079
77. Kalyuzhnyi S V (1997) BATCH ANAEROBIC DIGESTION OF GLUCOSE AND ITS MATHEMATICAL MODELING. II. DESCRIPTION, VERIFICATION AND APPLICATION OF MODEL. *Bioresour Technol* 59: 249–258
78. Mulrooney SB, Hausinger RP (2003) Nickel uptake and utilization by microorganisms. *FEMS Microbiol Rev* 27: 239–261. https://doi.org/10.1016/S0168-6445(03)00042-1
79. Ragsdale SW (2006) Nickel Enzymes & Cofactors. In: Encyclopedia of Inorganic Chemistry. *John Wiley & Sons*, pp 1–16
80. Yang Y, Zhang C, Hu Z (2013) Impact of metallic and metal oxide nanoparticles on wastewater treatment and anaerobic digestion. *Environ Sci Processes Impacts* 15: 39–48. https://doi.org/10.1039/c2em30655g
81. Mu H, Chen Y (2011) Long-term effect of ZnO nanoparticles on waste activated sludge anaerobic digestion. *Water Res* 45: 5612–5620. https://doi.org/10.1016/j.watres.2011.08.022

82. Li Q, Mahendra S, Lyon DY, et al (2008) Antimicrobial nanomaterials for water disinfection and microbial control: Potential applications and implications. *Water Res* 42: 4591–4602. https://doi.org/10.1016/j.watres.2008.08.015
83. Abdelsalam E, Samer M, Attia YA, et al (2016) Comparison of nanoparticles effects on biogas and methane production from anaerobic digestion of cattle dung slurry. *Renew Energy* 87: 592–598. https://doi.org/10.1016/j.renene.2015.10.053
84. Grosser A, Grobelak A, Rorat A, et al (2021) Effects of silver nanoparticles on performance of anaerobic digestion of sewage sludge and associated microbial communities. *Renew Energy* 171: 1014–1025. https://doi.org/10.1016/j.renene.2021.02.127

AIMS Press